Research on the Mechanics of CFRP Composite Lap Joints

by

Austin Curnutt

B.S., Kansas State University, 2017

A THESIS

submitted in partial fulfillment of the requirements for the degree

MASTER OF SCIENCE

Department of Architectural Engineering
College of Engineering

KANSAS STATE UNIVERSITY
Manhattan, Kansas

2017

Approved by:

Major Professor
Donald Phillippi, Ph.D., S.E., Architect

# Copyright

# Abstract

For this thesis, research was performed on CFRP bonded composite lap-joints with one and two continuous laminas through the lap. Composite wraps used to retrofit existing structures use lap joints to maintain their integrity. The use of composites for retrofitting structures has many advantages over traditional methods, such as steel jacketing, and is becoming more widely accepted in the structural engineering industry. While much literature exists documenting the performance of composite wraps as a whole when applied to concrete columns, less information is available on the behavior of the lap-joint of the wrap. Developing a better understanding of how the lap-joint behaves will help researchers further understand composite column wraps. This research sought to determine what affect continuous middle laminas may have on the stiffness of lap joints and whether or not stress concentrations exist in the lap-joint due to a change in stiffness.

# Table of Contents

# List of Figures

# List of Tables

# Acknowledgements

Thank you to Dr. Phillippi for his guidance through my entire graduate curriculum.

Thank you to Dr. Hayder Rasheed and Fred Hasler for their guidance as my committee members.

Thank you my family for always supporting me and helping me through school. Lastly, thank

you to Suzy for your support, love, and understanding as I went through this process.

# Symbols List

| | |
|---|---|
| $P$ | Applied load |
| $\Delta$ | Change in length |
| $L$ | Length |
| $A$ | Area |
| $E$ | Young's modulus |
| $\sigma$ | Stress |
| $\varepsilon$ | Strain |
| $n$ | Number of layers in lap |
| $\tau$ | Shear stress |
| $\lambda$ | Elongation parameter |
| $C_0$ | Adhesive stiffness parameter |
| $x$ | Location along lap |
| $c$ | Half of the lap length |
| $G_a$ | Adhesive shear modulus |
| $t_a$ | Adhesive thickness |
| $t_i$ | Inner adherend thickness |
| $t_o$ | Outer adherend thickness |
| $E_i$ | Inner adherend Young's modulus |
| $E_o$ | Outer adherend Young's modulus |
| $w_{avg}$ | Average width |
| $t_{avg}$ | Average thickness |
| $E_f$ | Fiber tensile Young's modulus |
| $E_m$ | Matrix tensile Young's modulus |
| $V_f$ | Fiber volume fraction |
| $V_m$ | Matrix volume fraction |
| $\sigma^T_{l,ult}$ | Ultimate tensile stress |

# Chapter 1 - Introduction

Bonded composites have been used extensively in the aerospace and defense industries since the 1940s and 50s. In the last three decades, civil and structural engineers have begun using them on structures as a means of retrofit. Many structures require retrofitting because of advances in the understanding of structural behavior during seismic events. Bonded composites are used in structures to strengthen slabs, beams, and columns. Other methods of retrofitting structures, such as steel jacketing of columns, have been around much longer in the field, but the use of composites has many advantages over other methods. Primarily, composites have a high strength-to-weight ratio, making them ideal for seismic retrofitting applications.

Composite wraps are often applied to columns to strengthen them against a seismic event. The wraps provide column confinement and increase column ductility. However, while much is known about the overall behavior of these column wraps, less information is available on the behavior of the lap-joints of the wraps. The lap-joint is the location where the composite wrap begins and ends. Composite wraps are often applied in many layers to a column without knowing the effect of multiple layers on lap-joint behavior. Single-lap joints have been the focus of many studies, dating back to the 1930s with Volkersen, but multi-lap joints have not been subject to investigation in the same frequency that single-lap joints have. Multi-lap joints are lap joints with one or more continuous layers through the joint. The purpose of this study is to better understand the effect of having one and two continuous layers through the lap on the stiffness of CFRP composite lap joints.

# Chapter 2 - Literature Review

Bonded composites have been in use for decades. During the second World War, the United States military began using glass fiber reinforced polymer composite vehicles in order to make the vehicles lighter and save steel (Palucka & Bensaude-Vincent, 2002). After World War II, the use of composites expanded into markets outside of the military. Beginning in the 1950's, composite materials experienced widespread use in the aerospace industry (Rasheed, 2015). Fiber reinforced polymers (FRP) were utilized to produce airplane and rocket components and motor casings. In addition to the aerospace industry, composites are used in the automotive, marine, offshore drilling, sporting equipment, and civil engineering industries. Within the civil engineering field, composite materials are often used to strengthen and retrofit reinforced concrete slabs, beams, and columns.

A composite material is a combination of two separate materials to form a single unit. The most commonly used composite material in civil engineering for retrofitting reinforced concrete structures is the polymer matrix composite. Polymer matrix composites consist of two primary ingredients: the matrix and the reinforcement (Kaw, 1997). Epoxy resin is the most common matrix. Glass fibers, carbon fibers, and aramid fibers can all be used as reinforcement in polymer matrix composites. The focus of this thesis will be on carbon fiber reinforced polymers because they are less costly than aramid fibers, stronger than glass fibers, and are the most frequently used type of fiber in the civil engineering industry.

Polymer matrix composites, henceforth known as composites, are an anisotropic material—the material properties are different in each direction of the material. This is the largest difference between composites and other materials, such as steel plates or bars. Steel plates are isotropic and have the same material properties (modulus of elasticity, allowable

stresses, etc.) in each direction. Additionally, anisotropic materials have 21 independent elastic constants in their stiffness matrix, while isotropic materials only have two, meaning it is much easier to establish the stress-strain relationship for any particular point in an isotropic material (Kaw, 1997).  The matrix and reinforcement of a composite are combined to form a lamina. A lamina is a single layer, or ply, and composites are typically constructed from multiple plies, which form a laminate.

There are many advantages to using composite materials to retrofit reinforced concrete columns over other options, such as steel jacketing. First, composite column wraps increase the column's ductility without making the column stiffer. Column ductility increases because of confinement provided by the wrap. Increasing column ductility without increasing stiffness is beneficial because during seismic events stiffer elements attract more load. Because composite wraps do not increase column stiffness, the column does not attract additional load. Another advantage associated with composite wraps is they don't appreciably increase a structure's weight. Composites have a high strength-to-weight ratio, which means they help strengthen structures without increasing their weight. This is important because if the weight of the structure increases, the seismic forces acting on the structure increase and the columns may have to be redesigned to make sure they can withstand the new lateral load.

There are two primary disadvantages when considering composite materials. The first being the relatively high cost associated with the material. The second being the perceived lack of durability. Composite materials need to be protected because they have effectively no resistance to the high temperatures associated with a fire. If a column wrap is exposed to flames, the matrix phase, or epoxy, will melt and the wrap will become ineffective. That being said, the

wrap may be replaced after a fire. Additionally, the composites should be protected from impact to avoid fiber breakage.

## 2.1. Single-lap Joints

Single-lap joints are created using an adhesive layer to connect two adherends. Figure 1 shows a typical single-lap joint. Adhesive bonding is an alternative to mechanical bonding that avoids the use of drilled holes and reduces stress concentrations (Tsai & Morton, 2010). However, stress concentrations do still exist at the end of each adherend. The two types of stresses occurring in an adhesively bonded joint are transverse normal tensile (peel) stress and shear stress.
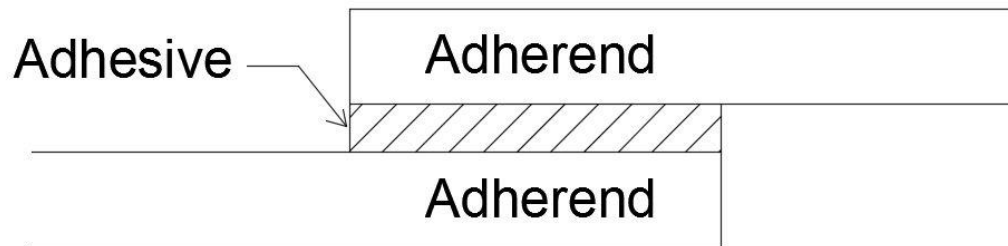


**Figure 1. Single-lap joint geometry**

Due to a sudden change in stiffness, stress concentrations occur at the lap location with the maximum stresses occurring at the overlap ends (Panigrahi & Pradhan, 2009). If a spew fillet is present at the ends of the adherends, the maximum adhesive stresses have been shown to be much lower than if the ends are squared off as they are in Figure 1 (Lempke, 2013). Figure 2 shows an example of a single-lap joint with a spew fillet on the adherend ends.
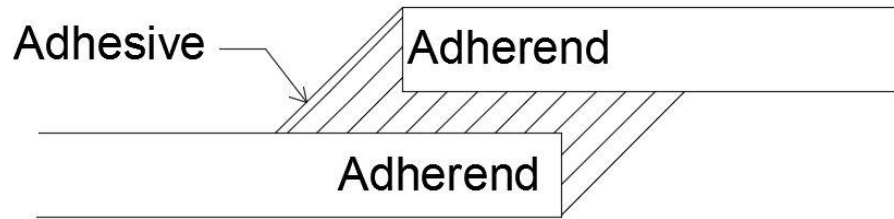
**Figure 2. Single-lap joint with spew fillet**

Several other parameters also have an impact on the stress distributions and strength of a single-lap joint. These parameters include the Young's Modulus, the shear modulus, and the Poisson's Ratios for the adherend and adhesive. The most efficient design of a single-lap joint is one such that the stiffness of each adherend is the same, meaning the joint is balanced. A balanced joint exhibits the lowest possible value of peak adhesive peel stress for any lap configuration (Kim & Kedward, 2002). Another factor affecting the stress distribution of the joint is the thickness of the adhesive. As the thickness of the adhesive increases, the stresses at the overlap ends increase (Lempke, 2013). This increase is because as the adhesive is made thicker, the eccentricity of the load is higher which increases the force on the bonding region of the single-lap joint. Additionally, increasing the Young's Modulus of the adhesive increases the stress at the overlap ends because the adhesive becomes stiffer and deforms less, which forces more stress and deformation into the adherends.

Adhesively bonded joints have two areas of concern. The bond shear strength, which is the load when shear failure occurs, and bond peel strength, which is the load when peel or tension failure occurs (Tong, 1996). Panigrahi and Pradhan (2009) found that in a single-lap joint, the adherends are likely to fail due to peel stresses before the adhesive layer fails. This is due to the low transverse tensile strength of a single-lap composite joint.

The two most widely used solutions for single-lap joints are the Volkersen solution and the Goland and Reissner solution. The first method for analyzing single-lap joints was proposed by Volkersen in 1938. He proposed a simple shear lag model based on the assumption of one-dimensional bar-like adherends with only shear deformation in the adhesive layer (Tsai, Oplinger, & Morton, 1998). The Volkersen model is based on five assumptions:

1) a constant bond and adherend thickness

2) uniform distribution of shear strain through the adhesive thickness

3) the adhesive carries only out-of-plane stresses while the adherends carry only in-plane stresses

4) linear elastic material behavior

5) deformation of the adherends in the out-of-plane direction is negligible

Goland and Reissner proposed their beam-on-elastic-foundation model in 1944. This model simulated the joint as being comprised of two beams bonded with a shear- and transverse normal-deformable layer (Tsai, Oplinger, & Morton, 1998). Tsai, Oplinger, and Morton (1998) were able to provide a better prediction of adhesive shear stress distribution than Goland and Reissner by including the adherend shear deformation in their analysis. The adherend shear deformation was accounted for in Tsai, Oplinger, and Morton's solution by assuming a linear shear stress through the adherend thickness.

During the 1970's, Hart-Smith developed an elastic-plastic model to predict the stresses in single-lap joints. In the research, Hart-Smith identified the strain energy density per unit bond area as the necessary parameter to establish the maximum bond strength achievable by the adhesive (Hart-Smith, 1973). Lempke (2013) discusses how, in the early 1990's, Tsai-Morton discovered that Hart-Smith's model was most accurate in predicting the stresses in short single-

lap joints. Short single-lap joints are defined as joints with a free adherend length to bonding length ratio of less than 0.75.

In 1996, Tong conducted a study into the bond strength for adhesively-bonded single-lap joints and found two main points. First, he showed that "the product of the strain energy density and the adhesive thickness is equal to the mixed-mode energy release rate for an adhesive bonded specimen." Second, he showed that "the strain energy density ratio is the same as the mode ratio of the mixed mode I and mode II fracture."

Strain energy density is a measure of the strain energy per unit of volume and is related to the stress and modulus of elasticity of the material. The energy release rate describes the rate at which a crack propagates through a solid material and is the sum of the energy needed to break the atomic bonds and the stored mechanical strain energy. For short crack lengths, the total energy of the object increases with an increasing crack length, meaning an increasing force must be acting on the object to grow the crack. Additional energy is required to be put into the object to lengthen the crack until the atoms become separated enough that they are no longer attracted to one another. For long cracks, an increase in crack length decreases the total amount of energy in the system, which means the crack grows without the application of additional force.

The modes of failure, referenced above, are referencing a laminate failure, or a failure occurring between the lamina. There are three modes of failure, as shown in Figure 3 below. Mode I failure occurs when the cracking plane occurs normal, or perpendicular, to the direction of tensile loading (*Fracture Toughness*). Mode II failure is present when a shear failure occurs between the lamina parallel to the direction of tensile loading. Mode III failure is present when out-of-plane sliding deformation occurs.
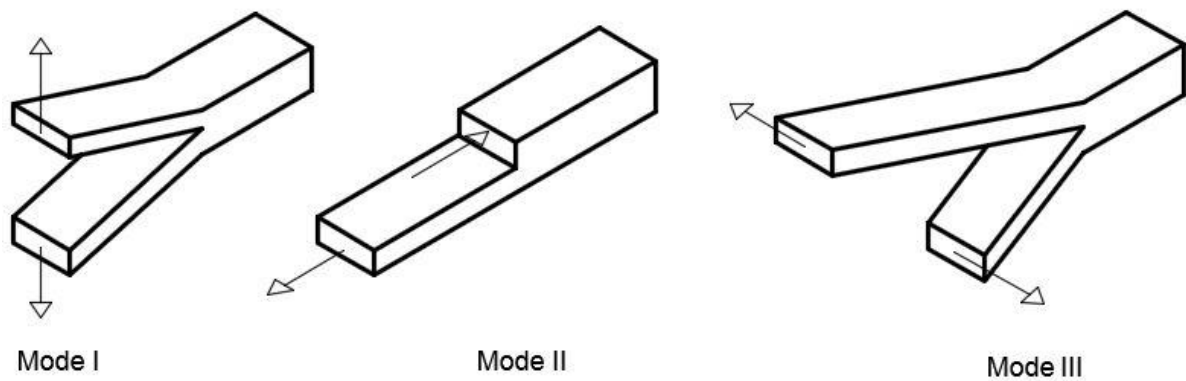
**Figure 3. Failure modes of laminate**

In addition to the three types of laminate failure, there are three types of lamina failure (Kaw, 1997). The three types of individual ply failure for a unidirectional lamina under longitudinal tensile loading, shown in Figure 4, are (1) brittle fracture of fibers, (2) brittle fracture of fibers with pullout, and (3) fiber pullout with fiber-matrix debonding. The type of failure depends on the bond strength between the fiber and the matrix and the fiber volume fraction. Brittle fracture of fibers occurs for low fiber volume fractions (less than 0.4); Brittle fracture with fiber pullout occurs for fiber volume fractions ranging from 0.4 to 0.65; and fiber pullout with debonding occurs when the fiber volume fraction is greater than 0.65. The fiber volume fraction is a ratio of the volume of the fibers to the total volume of the composite.
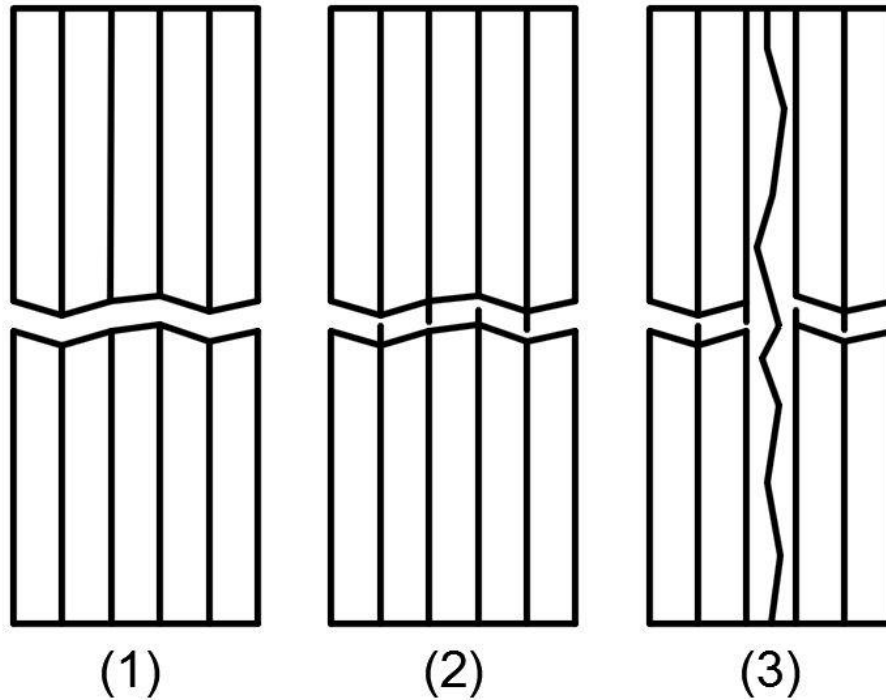
**Figure 4. Failure modes of unidirectional lamina in longitudinal tension**

Tong again performed a study in 1998 in which a solution predicting the strengths of adhesively bonded unbalanced single-lap joints with nonlinear adhesive properties was found. His procedure consisted of a global/local analysis similar to that developed by Goland and Reissner. Tong found that when subjected to a given load, the bond strain energy rate at the ends of the overlap can be computed in terms of the membrane forces and the bending moments. Overall, Tong showed that "neglecting the terms related to the transverse shear forces had a slight effect on predictions of both [shear and peel] strain energy rates when the adhesive is relatively flexible, and tended to yield a noticeable effect on both strain energy rates when the adhesive is relatively stiff."

## 2.2. Double-lap Joints

Double-lap joints are adhesive bonds in which two adherends are applied to either side of a central adherend, as shown in Figure 5. Similarly to single-lap joints, double-lap joints do not have uniform peel and shear stresses (Tong, Sheppard, & Kelly, 1996). The gradients of the stresses are steep near the ends of the joint and level out in the middle of the joint. Double-lap joints have four limiting stress criteria. The limiting stress criteria defined by Tong, Kuruppu, and Kelly (1997) are (1) adhesive shear failure, (2) adhesive peel failure, (3) interlaminar tensile failure, and (4) interlaminar shear failure. Among these four limiting criteria, interlaminar delamination of the surface ply appears to be the most common mode of failure for a composite-to-composite double-lap adhesively bonded joint (Tong, 2006). This interlaminar failure is believed to be caused due to a weakness in the through-the-thickness tensile strength of the composite adherend.
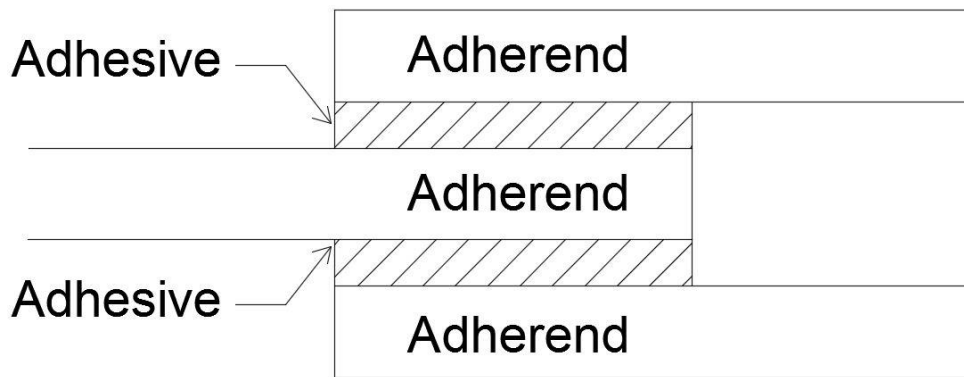


**Figure 5. Double-lap joint geometry**

The Volkersen/de Bruyne solution is the most commonly used method to analyze the stresses in a double-lap joint. De Bruyne developed this solution for the double-lap joint by using Volkersen's single-lap theory. The solution uses a shear-lag approach that models the adherends

as bars and the adhesive as a shear spring. In this solution, the assumption is made that the adherends do not have any shear deformation and that the adhesive layer carries only the shear stresses in order to transfer the longitudinal forces from the inner to the outer adherends (Tsai & Morton, 2010). Hart-Smith later showed that adhesive plasticity is a key player in determining the bond shear strength for double-lap joints (Tong, Kuruppu, & Kelly, 1997).

In the previously discussed double-lap joint analyses shear deformation of the adherends was ignored. However, large shear stresses would be present at the surfaces of the adherends next to the adhesive layer because the adhesive layer withstands large shear stresses during load transfer. The large shear stresses at the interface between the adhesive and adherend layers cause the adherend to undergo shear deformation (Tsai, Oplinger, & Morton, 1998). This is especially true for adherends with a low transverse shear modulus. Tsai, Oplinger, and Morton (1998) provided a solution that improves upon the Volkersen/de Bruyne theory by considering the adherend shear deformation in the analysis of double-lap joints by assuming a linear stress/strain through the thickness of the adherend. Additionally, Tsai, Oplinger, and Morton (1998) showed that for relatively large values of the transverse shear modulus and relatively small values of adherend thickness, the adherend shear deformations may be ignored and the Volkersen/de Bruyne solution reasonably predicts the adhesive shear stress.

In 2010, Tsai and Morton showed that the assumption of zero adherend shear stress made by the Volkersen/de Bruyne solution is not valid. Tsai and Morton showed that the Volkersen/de Bruyne solution predicted maximum shear stress values 33% higher than those found during their experiment (Tsai & Morton, 2010). Additionally, they showed that the Tsai, Oplinger, and Morton solution, discussed previously, provides a good prediction of the normalized adhesive shear strain distribution for both a unidirectional and a quasi-isotropic joint. Also documented

were the typical failure modes for the unidirectional and quasi-isotropic joints. Both joints were found to fail at the end of the strap with cohesive failure occurring in the unidirectional joint and delamination at the first ply occurring in the quasi-isotropic joint.

In 1994, Tong performed a study on double-lap joints and developed equations relating the maximum load that can be applied to the maximum strain energy density obtainable in shear in the adhesive (Tong, 1994). That study also showed that for stiffness balanced joints, shear failure occurs at both ends of the overlap. However, an imbalance in stiffness will cause the shear failure to occur at one end of the overlap, and, thus, decrease the overall bond strength of the joint. Another important parameter to consider is nonlinear adhesive behavior. This behavior becomes important when an applied load is large enough to create plastic zones at each end of the adhesive layer (Tong, Kuruppu, & Kelly, 1997). For composite double-lap joints, linear analyses predicted failure loads far less than those measured by Tong, Kuruppu, and Kelly (1997), while their nonlinear analysis seemed to give a good prediction of the failure load.

For the analysis of a more practical real world scenario, Tong, Sheppard, and Kelly (1996) investigated the effect of adherend alignment on the behavior of adhesively bonded double-lap joints. In the manufacturing of double-lap joints it is difficult to perfectly align the ends of the outer adherends. The analysis of end mismatch, as shown in Figure 6, showed that local bending is caused which, as described by Tong, "has an effect on the surface normal displacement of the outer adherend and stresses in the adhesive layer." An increase in peel stress due to the end mismatch is undesirable because it may cause premature failure of the joint. In order to account for end mismatch, Tong, Sheppard, and Kelly developed a modified formula that characterizes the peel stress in terms of surface normal displacement.
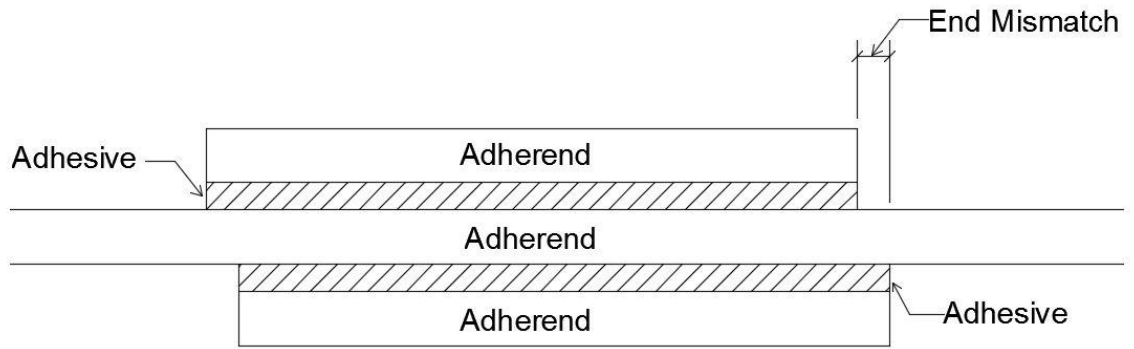
**Figure 6. Lap-joint with end mismatch**

# Chapter 3 - Experiment

## 3.1 Problem description

The situation explored for this thesis is a lap-joint with one and two continuous middle layers. Figure 7 shows a lap-joint with one continuous middle lamina and Figure 8 shows a lap-joint with two continuous laminas. These geometries require investigation because no previous experimentation has been done on a lap-joint with a similar geometry. The purpose of this investigation is to determine what effect the continuous middle lamina(s) may have on the stiffness of the lap-joint and if stress concentrations occur due to a change in stiffness at the lap joint.
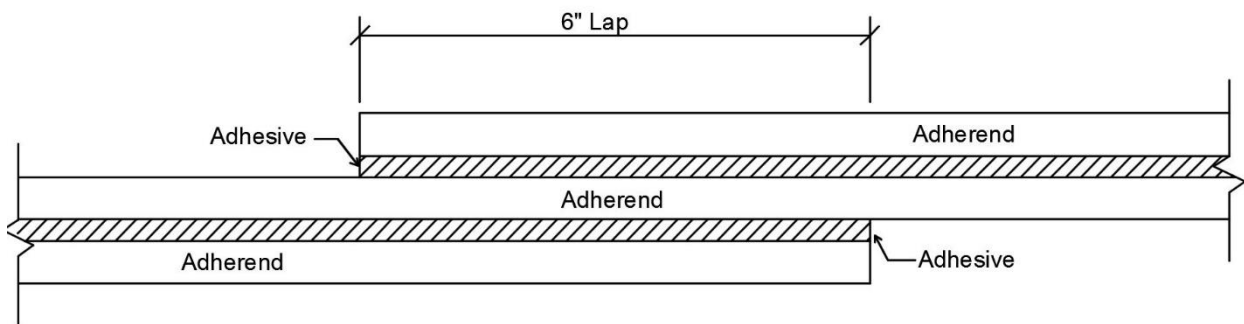


**Figure 7. Lap-joint with one continuous middle layer**
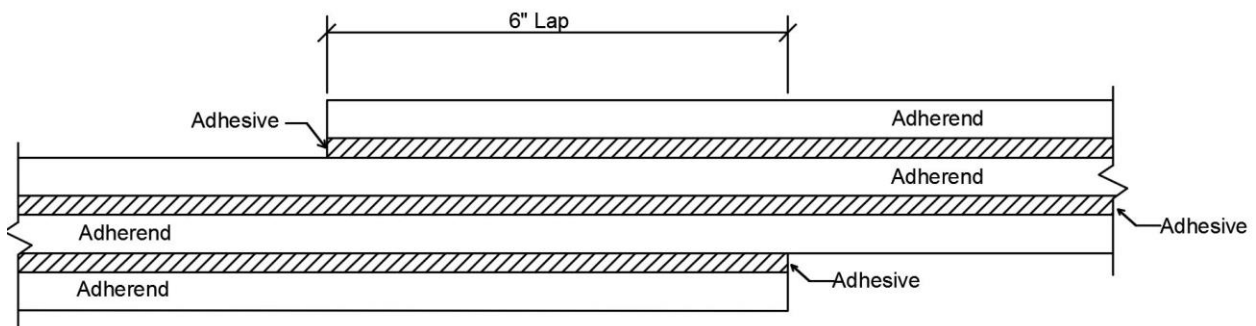


**Figure 8. Lap-joint with two continuous middle layers**

Carbon fiber reinforced polymer wraps are often used in civil engineering around reinforced concrete columns. In the field, a wrap will likely be applied continuously around the column multiple times. Understanding the actual stiffness of the lap-joint will play a crucial role in understanding the behavior of the interaction between the column and the wrap.

## 3.2 Specimen construction

Each individual strip that was tested was cut from a larger wrap. In total, nine wraps were created for use in this experiment. The wraps were formed around a wooden block three inches thick and twelve inches long. The flat length on the top and bottom of the block is nine inches. The block is shown in Figure 9 below.
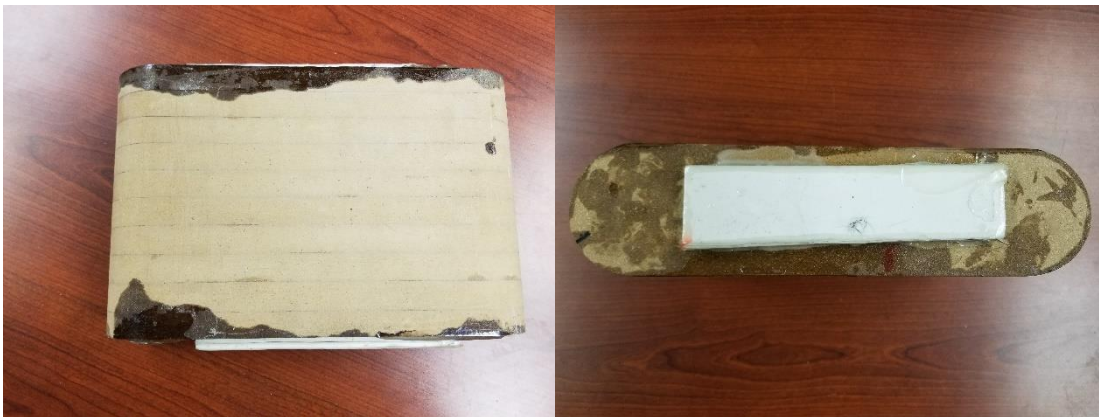


**Figure 9. Wood block used to form the CFRP wraps**

Plastic was wrapped around the block before the carbon fiber fabric was applied to aid in removing the wrap from the block once it finished curing. To begin construction of the wrap, the length of the carbon fiber was laid out on a table and saturated with neat resin, Figure 10 below. The carbon fiber fabric used for this experiment was SikaWrap Hex 230c. The neat resin used for this experiment was created by mixing three parts epoxy with one part hardener. The resin

was made using Fibre Glast 2000 Epoxy Resin with Fibre Glast 2060 Epoxy Cure. The

properties of the carbon fiber and epoxy are given in Section 4.3.



**Figure 10. Saturating the carbon fibers with neat resin**

After the end of the fabric was in place, the block was flipped length wise down the table

to apply the wrap, shown in Figures 11 and 12. The wrap was pulled snug onto the block to

minimize any imperfections.

**Figure 11. Flipping the block along the table to apply the fabric**



**Figure 12. Flipping the block along the table to apply the fabric**

Each specimen was constructed and left to cure in an outdoor environment. Three specimens were made in total. One specimen was made having no continuous layers through the lap, one specimen was made having one continuous layer through the lap, and one specimen was made having two layers continuous through the lap. The specimen with no continuous layer through the lap was made to be the control for the experiment. After each specimen cured completely it was removed from the block and cut into strips approximately one inch wide using

17

a tile saw, which can be seen in Figures 13 and 14 below.  Specimens were cut into one inch

strips to follow the requirements of ASTM D3039, described in section 3.4. Three single-lap

strips, five strips with one continuous layer, and five strips with two continuous layers were cut

and tested.



**Figure 13. Saw used to cut specimens**
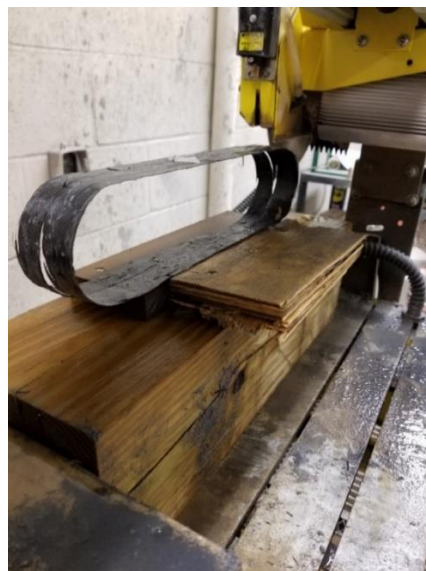


**Figure 14. Saw used to cut specimens**

## 3.3 Specimen properties

After cutting each specimen into strips, measurements were taken to determine an average width and thickness of the lap side and the back side of the specimen. The side with the lap joint is being called the lap side and the side opposite the lap-joint is considered as the back side. Averages were determined by taking measurements in three places along the lap and three places along the back side. The average measurements for each specimen are given in Table 1.

**Table 1. Average specimen measurements**

| Specimen | L.S. $w_{avg}$ (in) | B.S. $w_{avg}$ (in) | Lap $t_{avg}$ (in) | B.S. $t_{avg}$ (in) |
|----------|------------|------------|-----------|-----------|
| 0.1A | 0.903 | 0.881 | 0.052 | 0.025 |
| 0.2A | 0.925 | 0.973 | 0.034 | 0.046 |
| 0.3A | 0.97 | 1.06 | 0.056 | 0.059 |
| 0.4A | 0.891 | 0.867 | 0.044 | 0.051 |
| 1.1 | 0.965 | 0.923 | 0.088 | 0.047 |
| 1.3 | 0.87 | 0.983 | 0.103 | 0.058 |
| 1.4 | 1.007 | 0.845 | 0.091 | 0.053 |
| 1.5 | 0.797 | 0.919 | 0.092 | 0.046 |
| 1.6 | 0.957 | 0.877 | 0.076 | 0.058 |
| 2.1 | 1.027 | 0.976 | 0.121 | 0.055 |
| 2.2 | 1.147 | 1.041 | 0.133 | 0.082 |
| 2.3 | 0.735 | 0.895 | 0.132 | 0.083 |
| 2.4 | 0.852 | 1.009 | 0.127 | 0.063 |
| 2.6 | 0.926 | 0.977 | 0.122 | 0.075 |
| L.S. = Lap side | | | | |
| B.S.= Back side | | | | |
| w = Width | | | | |
| t = Thickness | | | | |

## 3.4 Test set-up

Each specimen was attached to two three inch diameter steel pins and tested in tension. One of the steel pins is shown in Figure 15. The strips were pulled at a displacement rate of 0.05 inches per minute in accordance with ASTM D3039. ASTM D3039 is the standard most

applicable to the testing performed for this experiment. The tests for this experiment were performed on continuous strips of a polymer matrix composite whereas ASTM D3039 is designed for tensile tests on polymer matrix composite coupons.

Each test was done on the MTS 810 Material Test System machine. During the test, strain gauges were placed in three locations. Strain gauge one was placed on the lap near the end; strain gauge two was placed on the lap side of the specimen outside of the lap; and, strain gauge three was placed on the back side of the specimen. Strain gauge locations are shown in Figure 18. The strain was used to determine the stiffness of the composite wrap as will be described in section 4.1.

A hollow metal tube was placed between each of the steel pins to limit inward rotation of the test specimen. In a real world application against a concrete column, the wrap will not be able to rotate inward towards its center because the concrete will be pushing it outward. The tube can be seen between the pins in Figure 16. An overall set-up of the experiment is shown in Figure 17.



**Figure 15. Steel pin used for tensile test**
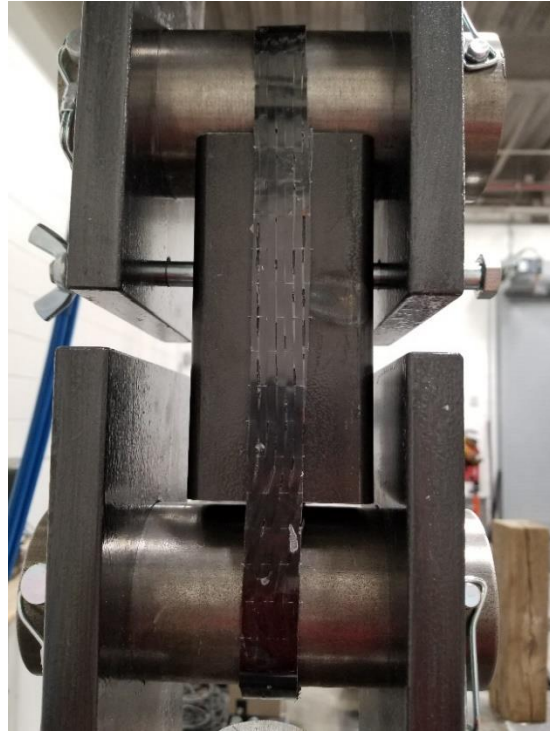
**Figure 16. Set-up showing tube in center**



**Figure 17. Test set-up**

# Chapter 4 - Theoretical Models

## 4.1 Stiffness equation model

The purpose of this research is to relate strain to an average stiffness, $K_{avg}$, in order to determine the stiffness of a CFRP wrap with a certain number of layers and a six inch lap length.
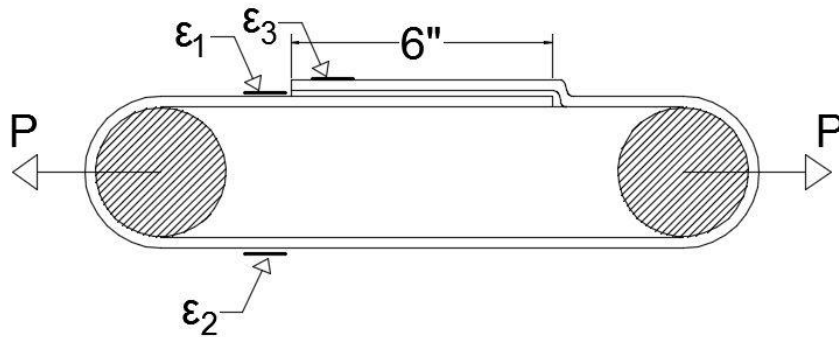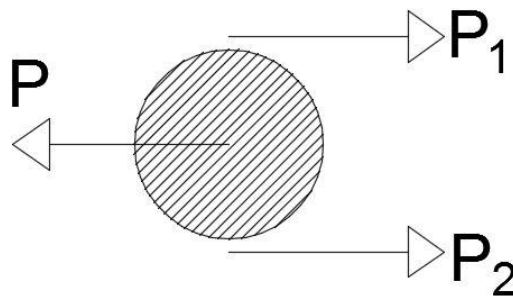


**Figure 18. Experimental set-up**



**Figure 19. Free body diagram of CFRP around pin**

From the free body diagram,

$$P = P_1 + P_2 \qquad (1)$$

For these calculations, it is assumed that compared to the rest of the strap, the elongation around the pins is relatively constant and therefore negligible. From this assumption, the change in length of the wrap is given by

$$\Delta_1 = \frac{P_1 L_1}{E_1 A_1} \tag{2}$$

$$\Delta_2 = \frac{P_2 L_2}{E_2 A_2} \tag{3}$$

where,
   $L_1$=total length minus the lap length, 3"
   $L_2$= total length, 9"

And, $A_1 \approx A_2$ and $E_1 \approx E_2$. From this relationship equation 3 can be rewritten as

$$\Delta_2 = \frac{P_2 L_2}{E_1 A_1} \tag{3.1}$$

The average stress over the section is given by

$$\sigma_1 = \frac{P_1}{A_1} \tag{4}$$

$$\sigma_2 = \frac{P_2}{A_2} = \frac{P_2}{A_1} \tag{5}$$

The stress over the section is also given by

$$\sigma_1 = E_1 \varepsilon_1 \tag{6}$$
$$\sigma_2 = E_1 \varepsilon_2 \tag{7}$$

By solving equations 4 and 5 for the force and substituting into equation 1:

$$P = \sigma_1 A_1 + \sigma_2 A_1 \tag{8}$$

From substituting equations 6 and 7 into equation 8 and simplifying, the following expression can be found for the total tensile force in the wrap.

$$P = E_1 A_1 (\varepsilon_1 + \varepsilon_2) \tag{9}$$

If area three is over the length of the lap, it follows that

$$P_1 = P_3 \tag{10}$$

$$\Delta_3 = \frac{P_3 L_3}{E_{avg} A_3} \tag{11}$$

where,
        $L_3$= length of the lap, 6"
        $E_{avg}$= average stiffness of the lap

From equation 10, it follows that

$$P_3 = E_1 \varepsilon_1 A_1 \tag{12}$$

By plugging equation 12 into equation 11 and rearranging, an expression for the average stiffness of the lap joint is given by equation 13.

$$\frac{E_{avg} A_3}{L_3} = k_{avg} = \frac{E_1 \varepsilon_1 A_1}{\Delta_3} \tag{13}$$

## 4.2 Modified Volkersen model

For the theoretical analysis the shear-lag based solution proposed by Volkersen was used with modifications to account for the middle continuous laminas. The equations used to determine the shear stress through the lap are given in equations 14 through 16. The number of layers through the lap is given by n. n should include both outer adherends and all of the inner adherends continuing through the lap. The (n-1) term was added to the elongation parameter, $\lambda^2$, and the $C_0$ equation. If the number of layers is input as two, i.e. no continuous lamina through the

lap, Volkersen's original equations are recovered. The terms related to the stiffness of the lap

joint are $C_0$ and $\lambda^2$. The purpose of the modified Volkersen model is to find a way to determine

the stiffness of the joint and match it with the stiffness given by equation 13.

$$\tau(x) = \lambda \left[ \left( \frac{P_x}{n} - \frac{C_0}{\lambda^2} \right) \frac{sinh(\lambda x)}{cosh(\lambda c)} + \frac{P_x}{n} \left( \frac{cosh(\lambda x)}{sinh(\lambda c)} \right) \right] \tag{14}$$

$$\lambda^2 = \frac{G_a}{t_a} \left( \frac{1}{E_o t_o} + \frac{1}{E_i t_i (n-1)} \right) \tag{15}$$

$$C_0 = \frac{G_a P_x}{E_i t_i (n-1) t_a t_o} \tag{16}$$

## 4.3 Specimen strength

Using the measurements listed in Table 1, the fiber volume fraction, matrix volume

fraction, tensile modulus, ultimate tensile stress, and maximum force were calculated for the lap

side and back side of each specimen. Each of the parameters listed was calculated using the

properties of the Sika 230C carbon fiber and Fibre Glass Series 2000 Epoxy, given in Tables 2

and 3.

**Table 2. Sika 230C carbon fiber properties**

| Primary fiber direction | 0° Unidirectional |
|---|---|
| Density | 0.065 #/in3 |
| Area weight | 0.0003279 #/in2 |
| Thickness per layer, $A_f$ | 0.005045 in |
| Tensile strength, $\sigma_{ult,}{}^t$ | 5 x 105 psi |
| Tensile elastic modulus, $E_f$ | 33.4 x 106 psi |
| Elongation, $\varepsilon_f$ | 0.015 in/in |

**Table 3. Fibre Glast Series 2000 Epoxy properties**

| Property | Neat Resin | With Carbon |
|---|---|---|
| Density | 0.0401 lb/in$^3$ | |
| Tensile Strength, $\sigma_{f,ult}^{T}$ | 9828 psi | -- |
| Elongation at Break, $\varepsilon$ | 0.019 in/in | 0.0091 in/in |
| Tensile Modulus, $E_m$ | 418,525 psi | -- |

The amount of fiber is determined by the thickness per layer of carbon fiber multiplied by the number of layers in the lap or back side. The fiber volume fraction is the thickness of the fiber present divided by the average thickness of the location. The matrix volume fraction is one minus the fiber volume fraction. The composite tensile modulus was calculated using equation 17, the composite ultimate tensile stress was calculated using equation 18, and the maximum force was calculated using equation 19. The results of the calculations are given in Table 4 for the lap side of the specimen and Table 5 for the back side of the specimen.

$$E_L = E_f V_f + E_m V_m \tag{17}$$
$$\sigma_{l,ult}^{T} = \sigma_{ult,t} V_f + \varepsilon_{min} E_m V_m \tag{18}$$
$$F = \sigma_{l,ult}^{T} w_{avg} t_{avg} \tag{19}$$

**Table 4. Lap side composite calculations**

| Specimen | Average Width (in) | Average thickness (in) | Layers of Carbon | Fiber Volume Fraction | Matrix Volume Fraction | Tensile Modulus (psi) | Ultimate Tensile Stress (psi) | Maximum Force (lbs) |
|---|---|---|---|---|---|---|---|---|
| | | | | Lap | | | | |
| 0.2A | 0.925 | 0.034 | 2 | 0.297 | 0.703 | 10,206,245.15 | 151,061 | 4,751 |
| 0.3A | 0.97 | 0.056 | 2 | 0.180 | 0.820 | 6,361,059.55 | 93,211 | 5,063 |
| 0.4A | 0.891 | 0.044 | 2 | 0.229 | 0.771 | 7,981,757.61 | 117,594 | 4,610 |
| 1.1 | 0.965 | 0.088 | 3 | 0.172 | 0.828 | 6,090,943.21 | 89,148 | 7,570 |
| 1.3 | 0.87 | 0.103 | 3 | 0.147 | 0.853 | 5,264,859.25 | 76,720 | 6,875 |
| 1.4 | 1.007 | 0.091 | 3 | 0.166 | 0.834 | 5,903,939.59 | 86,334 | 7,911 |
| 1.5 | 0.797 | 0.092 | 3 | 0.165 | 0.835 | 5,844,315.24 | 85,437 | 6,265 |
| 1.6 | 0.957 | 0.076 | 3 | 0.199 | 0.801 | 6,986,592.14 | 102,622 | 7,464 |
| 2.1 | 1.027 | 0.121 | 4 | 0.167 | 0.833 | 5,919,050.99 | 86,562 | 10,757 |
| 2.2 | 1.147 | 0.133 | 4 | 0.152 | 0.848 | 5,422,760.68 | 79,095 | 12,066 |
| 2.3 | 0.735 | 0.132 | 4 | 0.153 | 0.847 | 5,460,671.74 | 79,666 | 7,729 |

**Table 5. Back side composite calculations**

| Specimen | Average Width (in) | Average thickness (in) | Layers of Carbon | Fiber Volume Fraction | Matrix Volume Fraction | Tensile Modulus (psi) | Ultimate Tensile Stress (psi) | Maximum Force (lbs) |
|---|---|---|---|---|---|---|---|---|
| | | | | Back side | | | | |
| 0.2A | 0.973 | 0.046 | 1 | 0.110 | 0.890 | 4,035,710.16 | 58,228 | 2,606 |
| 0.3A | 1.06 | 0.059 | 1 | 0.086 | 0.914 | 3,238,697.75 | 46,237 | 2,892 |
| 0.4A | 0.867 | 0.051 | 1 | 0.099 | 0.901 | 3,681,081.72 | 52,892 | 2,339 |
| 1.1 | 0.923 | 0.047 | 2 | 0.215 | 0.785 | 7,498,996.49 | 110,331 | 4,786 |
| 1.3 | 0.983 | 0.058 | 2 | 0.174 | 0.826 | 6,156,143.71 | 90,129 | 5,139 |
| 1.4 | 0.845 | 0.053 | 2 | 0.190 | 0.810 | 6,697,430.85 | 98,272 | 4,401 |
| 1.5 | 0.919 | 0.046 | 2 | 0.219 | 0.781 | 7,652,920.33 | 112,647 | 4,762 |
| 1.6 | 0.877 | 0.058 | 2 | 0.174 | 0.826 | 6,156,143.71 | 90,129 | 4,584 |
| 2.1 | 0.976 | 0.055 | 3 | 0.275 | 0.725 | 9,494,409.14 | 140,351 | 7,534 |
| 2.2 | 1.041 | 0.082 | 3 | 0.185 | 0.815 | 6,506,000.03 | 95,392 | 8,143 |
| 2.3 | 0.895 | 0.083 | 3 | 0.182 | 0.818 | 6,432,656.66 | 94,289 | 7,004 |

# Chapter 5 - Results and Conclusion

## 5.1 Results

### 5.1.1 Experimental results

The data received from the testing machine used in the experiment was the total force the machine was pulling with, the total displacement of the pulling apparatus, and the strain for all three strain gauges. With the data provided from the machine, charts plotting force vs. displacement, lap strain vs. displacement, off lap strain vs. displacement, and back side strain vs. displacement were created. An example of these charts is shown below, in Figures 20 and 21.
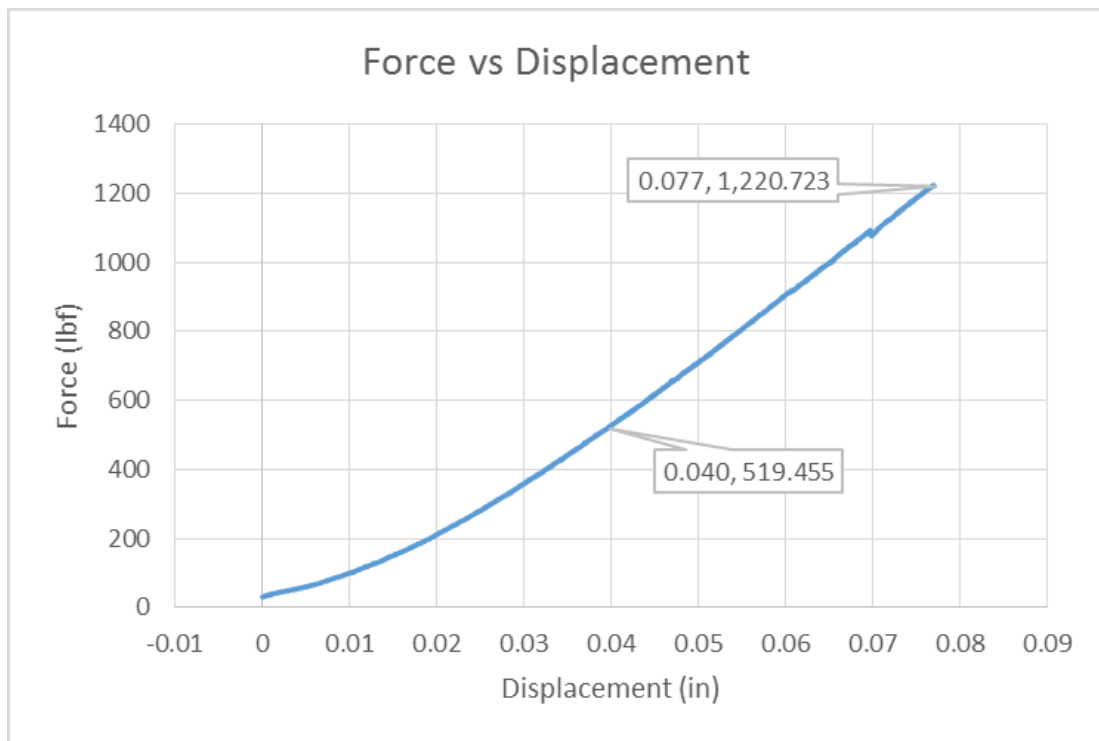
**Figure 20. Example of force vs. displacement chart using test data**
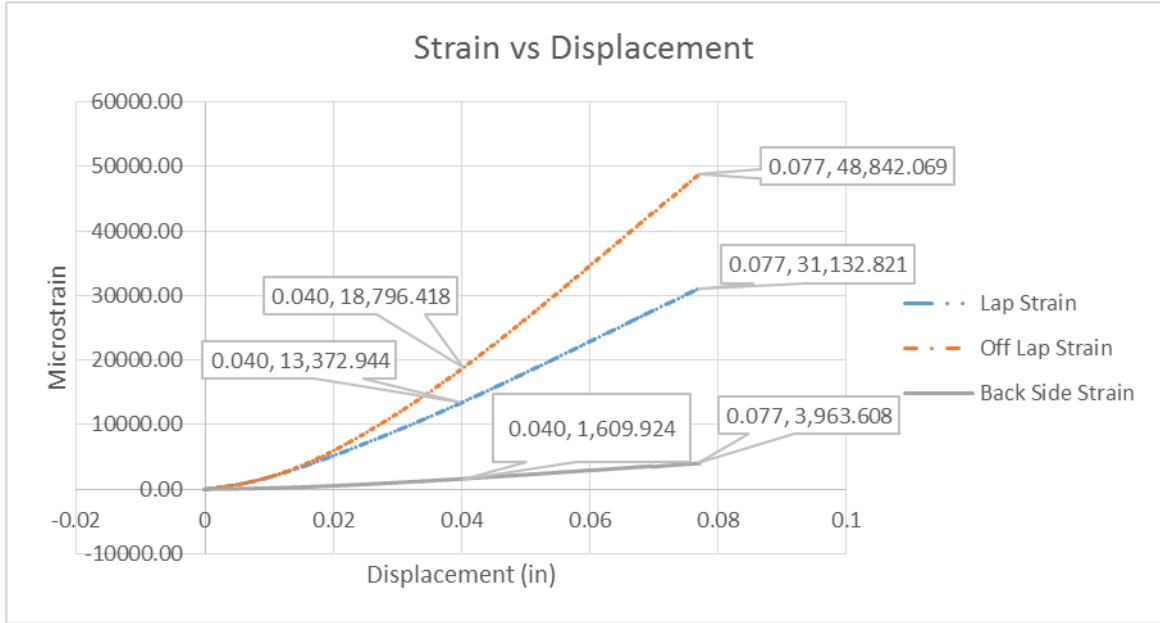
**Figure 21. Example of strain vs. displacement chart using test data**

From the charts above, two points of displacement were chosen from the linear portion of the graph. The two strains were chosen from the elastic portion of the graph to set the difference in the chosen strains as the true strain for the specimen at that location. Then, calculations were done to determine the forces $P_1$ and $P_2$ distributed to the off lap and back side, respectively, using the following equations.

$$\varepsilon_1 = \varepsilon_{1j} - \varepsilon_{1i} \tag{20}$$

$$\varepsilon_2 = \varepsilon_{2j} - \varepsilon_{2i} \tag{21}$$

$$P_1 = \frac{\varepsilon_1 A_1}{\varepsilon_1 A_1 + \varepsilon_2 A_2} P \tag{22}$$

$$P_2 = \frac{\varepsilon_2 A_2}{\varepsilon_1 A_1 + \varepsilon_2 A_2} P \tag{23}$$

The lap stress was calculated using $P_1$ divided by the average area of the lap, and then plotted on a stress vs. strain chart. The off lap stress was calculated using $P_1$ divided by the off lap average area, and the back side stress was calculated using $P_2$ and the average area of the back side. Examples of the stress vs. strain charts are shown below, in Figure 22. From these

29

charts, the modulus of each area was determined using the slope of the chart from the linear portion. Some of the charts have a portion of their strain data points in the negative region, as seen in the example of off lap stress vs. strain chart. This is believed to be caused by curvature at the lap joint. The lap joint is likely rotating outward, putting the surface in compression until the overall tension force through the lap became high enough to overcome the compression. A summary of the experimental tensile modulus results is given in Table 6, a summary of the maximum forces is presented in Table 7, a summary of the stress and microstrain at the breaking point is shown in Table 8, and all of the stress vs. strain charts for the specimens can be found in Appendix A.
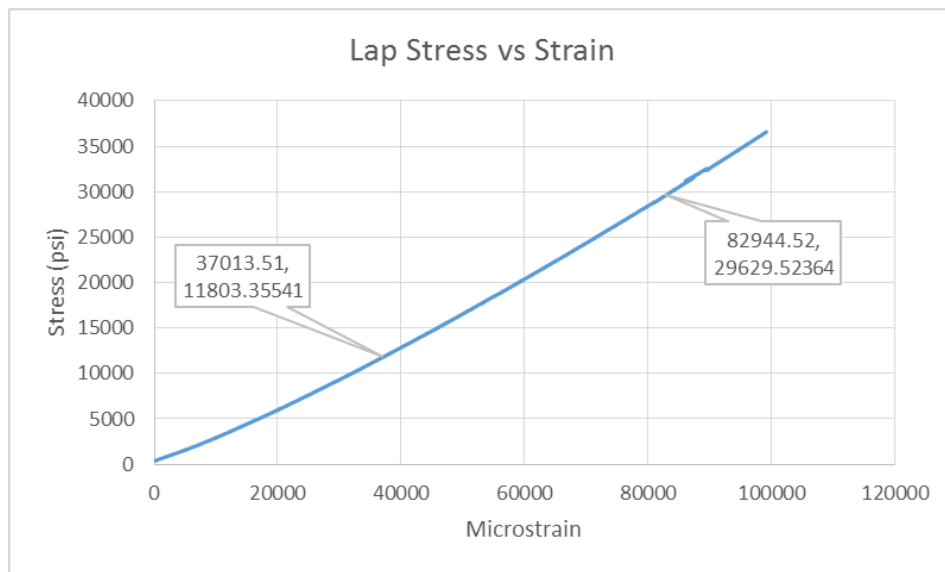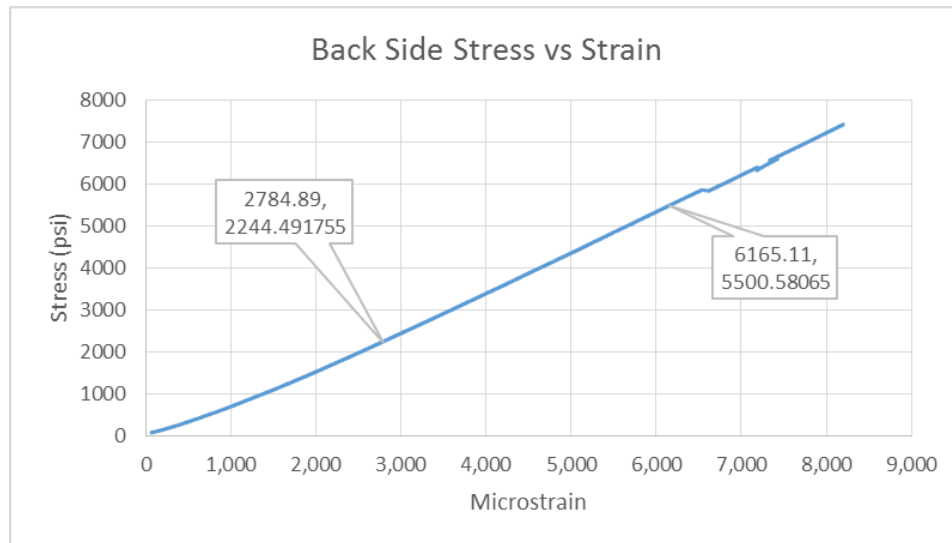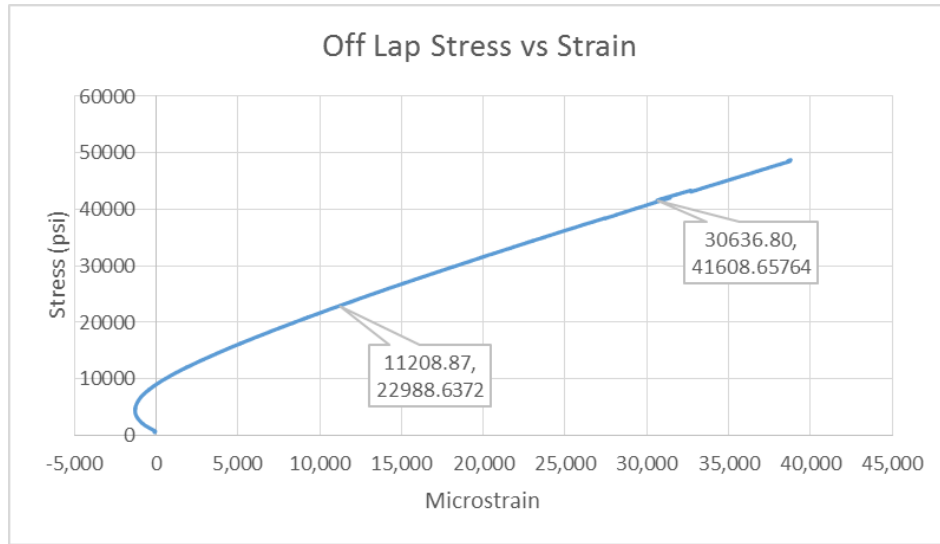
**Figure 22. Example stress vs. strain curves**

**Table 6. Summary of experimental tensile modulus**

| Specimen | Modulus (psi) | | |
|---|---|---|---|
| | Lap | Off Lap | Back Side |
| 0.2A | 1,136,347 | 640,055 | 612,765 |
| 0.3A | 758,396 | 469,153 | 275,207 |
| 0.4A | 820,154 | 469,411 | 460,129 |
| 1.1 | 387,497 | 954,825 | 998,123 |
| 1.3 | 101,767 | 569,292 | 564,804 |
| 1.4 | 131,885 | 813,547 | 857,701 |
| 1.5 | 249,803 | 1,213,997 | 1,166,175 |
| 1.6 | 178,618 | 811,830 | 795,428 |
| 2.1 | 352,563 | 471,492 | 474,449 |
| 2.2 | 567,461 | 349,704 | 342,394 |
| 2.3 | 269,655 | 491,899 | 512,094 |

**Table 7. Summary of experimental maximum forces**

| Specimen | At breaking point | |
|---|---|---|
| | Lap Side | Back Side |
| | $P_{1max}$ (lbf) | $P_{2max}$ (lbf) |
| 0.2A | 1104.65 | 115.89 |
| 0.3A | 1511.25 | 97.57 |
| 0.4A | 1029.70 | 90.65 |
| 1.3 | 219.56 | 1891.48 |
| 1.4 | 435.76 | 3361.38 |
| 1.5 | 579.61 | 2868.37 |
| 1.6 | 442.55 | 2798.88 |
| 2.1 | 4711.13 | 2493.01 |
| 2.2 | 4858.80 | 3238.07 |
| 2.3 | 3698.61 | 4010.69 |

**Table 8. Summary of experimental maximum stresses and microstrains**

| Specimen | Total Force (lbf) | Displacement (in) | Lap Peak Stress (psi) Microstrain | Off Lap Peak Stress (psi) Microstrain | Back Side Peak Stress (psi) Microstrain |
|---|---|---|---|---|---|
| | | | At breaking point | | |
| 0.2A | 1220.54 | 0.0771 | 35,124 | 33,173 | 2,589 |
| | | | 31,191 | 48,960 | 3,945 |
| 0.3A | 1608.81 | 0.0936 | 27,821 | 33,149 | 1,560 |
| | | | 33,918 | 71,569 | 5,316 |
| 0.4A | 1120.35 | 0.0762 | 26,265 | 28,892 | 2,050 |
| | | | 32,641 | 67,204 | 4,384 |
| 1.1 | 3430.09 | 0.1027 | 36,602 | 48,802 | 7,419 |
| | | | 99,238 | 38,791 | 8,199 |
| 1.3 | 2111.04 | 0.0720 | 2,450 | 3,321 | 33,176 |
| | | | 14,177 | 6,274 | 69,980 |
| 1.4 | 3797.14 | 0.1123 | 4,755 | 6,459 | 75,056 |
| | | | 35,226 | 7,813 | 90,779 |
| 1.5 | 3447.98 | 0.1309 | 7,905 | 9,962 | 67,852 |
| | | | 7,040 | 8,571 | 58,603 |
| 1.6 | 3241.43 | 0.0914 | 6,085 | 5,854 | 55,025 |
| | | | 24,977 | 7,660 | 73,912 |
| 2.1 | 7204.14 | 0.1455 | 37,911 | 40,595 | 46,442 |
| | | | 107,622 | 58,074 | 105,499 |
| 2.2 | 8096.87 | 0.1341 | 31,850 | 35,301 | 37,933 |
| | | | 38,404 | 103,137 | 112,704 |
| 2.3 | 7709.30 | 0.1560 | 38,122 | 38,413 | 53,991 |
| | | | 129,313 | 26,086 | 108,026 |

In order to determine the stiffness of each lap joint, an adjusted stress had to be calculated by using an adjusted strain for the off lap strain gauge. An adjustment was made because bending in the joint was causing forces which were either increasing or decreasing the value of the strain from the normal stress. For specimens 0.2A, 0.3A, and 0.4A the off lap strain gauge was placed in the tension region caused by the outward rotation of the joint. For these specimens, the strain at the maximum load had to be reduced because the tension force from bending was increasing the normal tensile force on the cross section. For specimens 1.3, 1.4, 1.5, 1.6, 2.1, 2.2, and 2.3 the off lap strain gauge was placed in the compression region caused by outward rotation

at the joint. For these specimens, the strain at the maximum load had to be increased because the compression force from bending decreased the normal tensile force. The strain of specimen 1.1 made it an outlier and it was ignored for all calculations. The adjusted strain at the specimen breaking point was calculated using the following equations.

$$e = 0.145t_{off\ lap} \tag{24}$$

$$M = eP_{1,max} \tag{25}$$

$$\sigma_{adjusted} = \frac{P_{1,max}}{A_{off\ lap}} + \frac{M}{S} \tag{26.1}$$

$$\sigma_{adjusted} = \frac{P_{1,max}}{A_{off\ lap}} - \frac{M}{S} \tag{26.2}$$

$$\varepsilon_{1,adjusted} = \varepsilon_1 \left(\frac{\sigma_{adjusted}}{\sigma}\right) \tag{27}$$

The value for the eccentricity of the load, e, was determined based on a ratio of an assumed distance between the centerlines of the outer adherends and the thickness of the specimen at the off lap joint. Equation 26.1 was used to determine the adjusted stress for specimens 1.3, 1.4, 1.5, 1.6, 2.1, 2.2, and 2.3; and equation 26.2 was used to calculate the adjusted stress for specimens 0.2A, 0.3A, and 0.4A.

From the adjusted strain on the lap side, the average stiffness of the lap was calculated using equations 28 and 13.1, where $L_1$ is assumed to equal three inches and $L_2$ is assumed to equal nine inches.

$$\Delta_3 = \Delta_2 - \Delta_1 = \varepsilon_2 L_2 - \varepsilon_{1,adjusted} L_1 \tag{28}$$

$$\left(\frac{EA_3}{L_3}\right)_{avg} = \frac{E_1 \varepsilon_{1,adjusted} A_1}{\Delta_3} \tag{13.1}$$

The value of $E_1$ used for the above calculation is the value listed for the off lap modulus in Table 6. When comparing the value of the modulus determined from experimental data, in Table 6, with the value of the modulus when calculating it from the manufacturer's data, in Table

4, it is clear to see that the experimental modulus is much lower. The difference in these values is likely due to imperfect construction in less than ideal conditions. A summary of the lap average stiffness is given after the discussion of the results from the modified Volkersen model.

### 5.1.2 Modified Volkersen model results

Using the equations given in Section 4.2, the value of the shear stress in the adhesive was calculated at discrete points along the lap and plotted as a function of distance from the centerline, as shown in Figure 23. The force used in the stress calculations was $P_{1,max}$ ,from the experimental results.  $P_{1,max}$ was divided by the total thickness of the lap. From Figure 23, the area under the curve was calculated from the peak to the point at which the stress is zero. The area under the curve is the total force transferred through the adhesive into the lap region. It can be seen from the figure that the adhesive almost fully transfers the load to the outer adherend of the lap after only about one half inch. For all of the specimens the area under the graph became zero at a distance of just over one inch. Using the area under the curve and dividing it by the distance along the curve until the stress is zero gives the maximum stiffness of the lap. Figure 24 shows an example of the stiffness of the lap determined using Figure 23. The average stiffness, shown in Figure 24, was determined by dividing the area under the curve of the actual stiffness by the total lap length of six inches. Charts of each specimen's adhesive shear stress distribution and average stiffness are given in Appendix B.
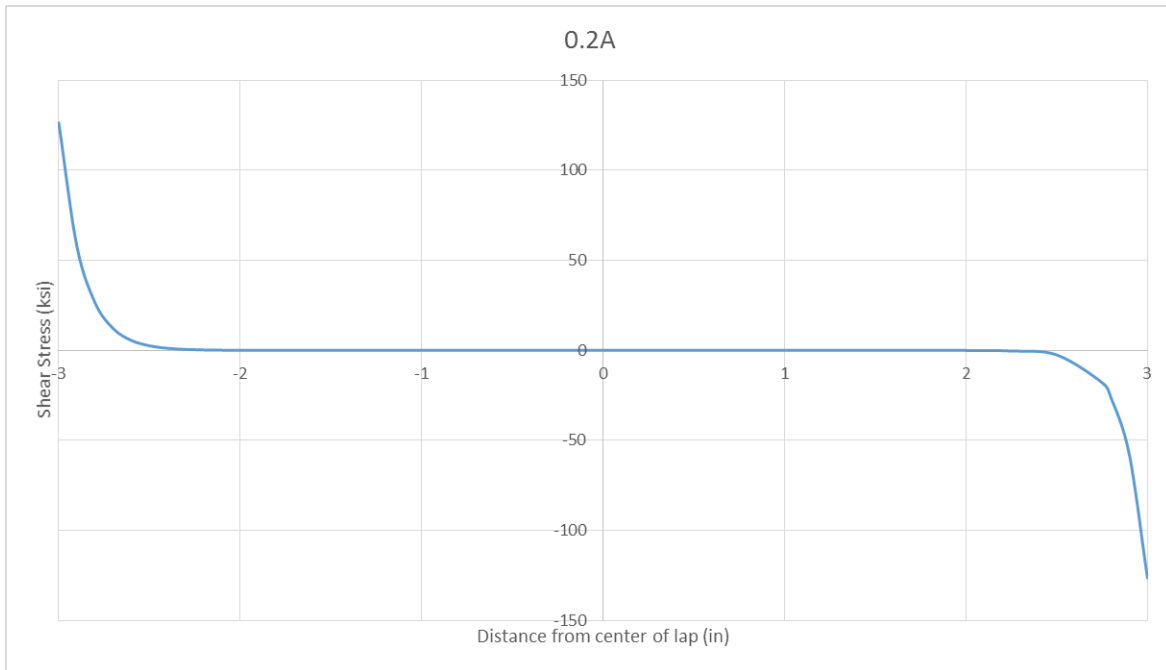
**Figure 23. Example plot of adhesive shear stress vs. distance from the lap center point**
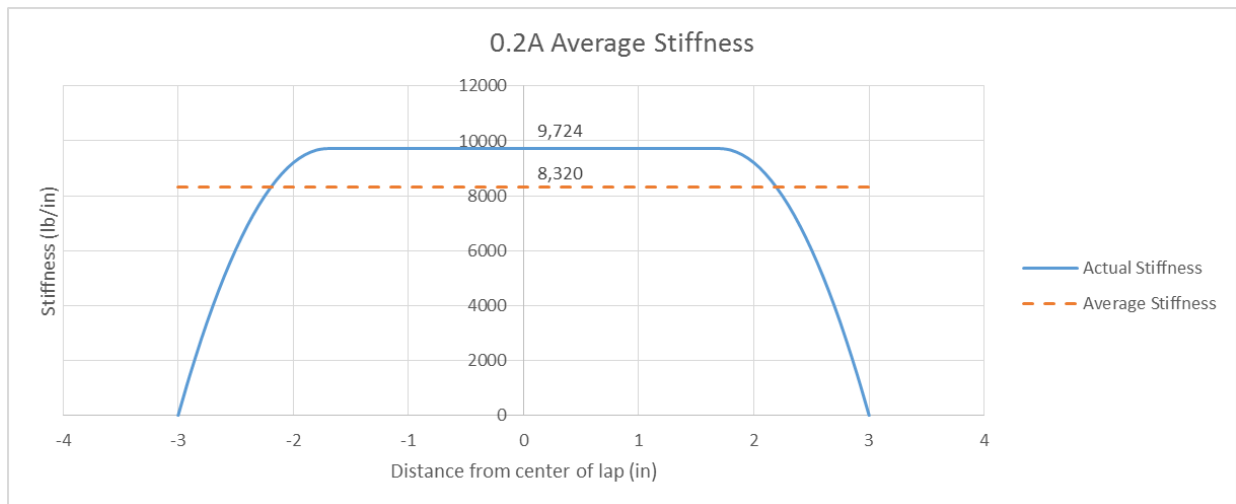


**Figure 24. Example plot of lap stiffness calculated from modified Volkersen model**

Table 9 gives a summary of the average stiffness of the lap joint determined by the experiment compared to that determined using the modified Volkersen model. It is obvious from the table that discrepancies exist between the results of the experiment and the results from the

36

modified Volkersen model. From this comparison, it is evident that additional investigation should be conducted in order to more consistently match theoretical models with the actual behavior of the composite wraps at the lap joint.

**Table 9. Comparison of experimental and modified Volkersen model average stiffness**

| Specimen | Average Stiffness (lb/in) | |
|---|---|---|
| | Experimental Results | Modified Volkersen Model |
| 0.2A | 68,207 | 8,320 |
| 0.3A | 70,749 | 5,296 |
| 0.4A | 67,289 | 5,425 |
| 1.3 | 433 | 237 |
| 1.4 | 560 | 595 |
| 1.5 | 1,268 | 754 |
| 1.6 | 776 | 785 |
| 2.1 | 12,155 | 3,488 |
| 2.2 | 7,215 | 3,154 |
| 2.3 | 6,747 | 2,369 |

## 5.2 Reasons for error and recommendations for future research

One potential source of error for this experiment is the assumption that the elongation of the strap around the pins of the testing apparatus was constant. Due to a high volume of specimen failure at the pin, it is likely that the elongation of the wrap around the pin was not constant and created areas of weakness. Another source of error is the assumption that no shear deformations exist in the layers. Shear deformations almost certainly exist in the adhesive layers and have an effect on the stiffness of the lap joint. An additional source of error arises from the assumption that the strain across the area is uniform. If the strain isn't uniform across the area then the stiffness across the area may not be uniform as well. Another source of error could be inconsistencies in the sizes of the specimens due to the cutting process. Not all of the specimens

are the same width and not all of the specimens with the same number of lamina are the same thickness due to the buildup of excess epoxy on the wraps.

Possible future research into multi-lap joints could include investigating different lap lengths and their effect on joint stiffness and stress distribution. Additional research could also be conducted on multi-layer laps using different models, such as the Hart-Smith Elastic-Plastic model. Further research could also be conducted into the effect shear deformation within the adhesive has on the joint stiffness. Another topic of future research could be additional modifications to the Volkersen model with the modifications being included in the derivation of the equations, rather than substituting a modification into the final equations. Lastly, once experimental results have been successfully matched with theoretical model results the next step would be to apply the composite to concrete cylinders to see if the behavior of the composite is changed because of its application to concrete.

## 5.3 Conclusion

Composite lap joints are important for the civil engineering industry. They are present when concrete columns in existing structures have been retrofitted for better seismic performance by applying a composite wrap. While using CFRP composite wraps is a popular method for retrofitting reinforced concrete columns and much is known about their overall behavior, less information is available on how multi-layer lap joints effect the behavior of the wrap. Wrapping layers of fabric around the column multiple times creates a multi-lap joint between the beginning and termination of the wrap.

The subject of this research was lap joints with multiple continuous laminas through the lap. The aspect of interest for this investigation was determining the stiffness of the lap joint in

order to examine how stress concentrations may affect the joint. To determine the stiffness of lap joints with zero, one, and two continuous laminas through the lap, tests were performed on specimens constructed of carbon fiber and epoxy. From these tests, experimental values of the average stiffness of the lap joint for each configuration were calculated and compared to a theoretical model that was intuitively modified to account for the continuous layers through the lap. While no definitive conclusion could be drawn from the study performed, results of this study may be used by future researchers to refine the equations presented so that a computational model can be formulated that accurately predicts actual lap behavior.

# References

Hart-Smith, L.J. (1973). Adhesive-bonded double-lap joints. NASA CR-112235

*Fracture Toughness.* Retrieved from https://www.nde- ed.org/EducationResources/
CommunityCollege/Materials/Mechanical/FractureToughness.php

Kaw, A. (1997). *Mechanics of Composite Materials.* Boca Raton, FL: CRC Press.

Kim, H., & Lee, J. (2004). Adhesive nonlinearity and the prediction of failure in bonded
composite lap joints. *Joining and Repair of Composite Structures, ASTM STP 1455,* K.T.
Kedward and H. Kim, Eds., ASTM International, West Conshohocken, PA.

Lempke, M (2013). *A study of single-lap joints* (Master's thesis, Michigan State University).
Retrieved from https://d.lib.msu.edu/etd/2280/datastream/OBJ/download/A_study_of_single-
lap_joints.pdf

Palucka, T., & Bensaude-Vincent, B. (2002, October 19). *Composites Overview.* Retrieved from
http://authors.library.caltech.edu/5456/1/hrst.mit.edu/hrs/materials/public/composites/Comp
osites_Overview.htm

Rasheed, H. A. (2015). *Strengthening design of reinforced concrete with FRP.* Boca Raton, FL:
CRC Press.

Tong, L. (2006). An analysis of failure criteria to predict the strength of adhesively bonded
composite double lap joints.

Tong, L., Kuruppu, M., & Kelly, D. (1997). Analysis of adhesively bonded composite double lap
joints. *Journal of Thermoplastic Composite Materials, 10*, 61-75.

Tong, L (1994). Bond shear strength for adhesive bonded double-lap joints. *International
Journal of Solids Structures,* 31, 2919-2931.

Tong, L (1996). Bond strength for adhesive-bonded single-lap joints. Acta Mechanica, 117, 101-
113.

Tong. L., Sheppard, A., & Kelly, D. (1996). Effect of adherend alignment on the behavior of
adhesively bonded double lap joints. *International Journal of Adhesion & Adhesives, 16*,
241-247.

Tong, L., Sheppard, A., & Kelly, D. (1995). Relationship between surface displacement and
adhesive peel stress in bonded double lap joints. *International Journal of Adhesion and
Adhesives, 15*, 43-48.

Tong, L. (1998). Strength of adhesively bonded single-lap and lap-shear joints. *International
Journal of Solids Structures,45*, 2601-2616.

Tsai, M.Y., & Morton, J. (2010). An investigation into the stresses in double-lap adhesive joints with laminated composite adherends. *International Journal of Solids and Structures, 47*, 3317-3325.

Tsai, M.Y., Oplinger, D.W., & Morton, J. (1998). Improved theoretical solutions for adhesive lap joints. *International Journal of Solids Structures, 35*, 1163-1185.

# Appendix A - Experiment Results

The tensile moduli listed in Table 6 were calculated for each specimen using the graphs below. The tensile modulus is the slope between the two points shown on the graph.

**Specimen 0.2A**
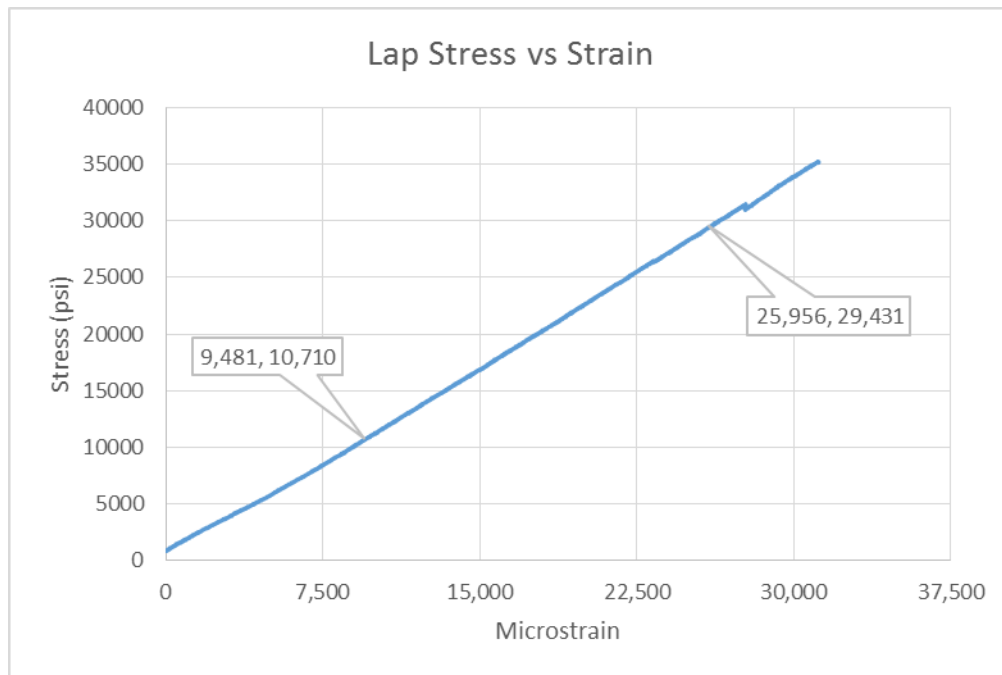


**Figure 25. 0.2A lap test result**
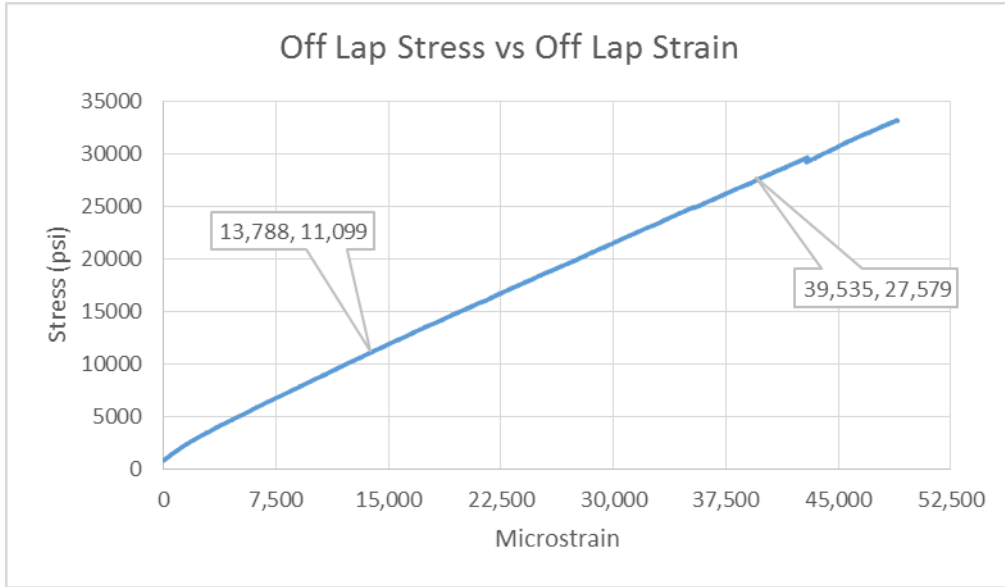
**Figure 26. 0.2A off lap test result**
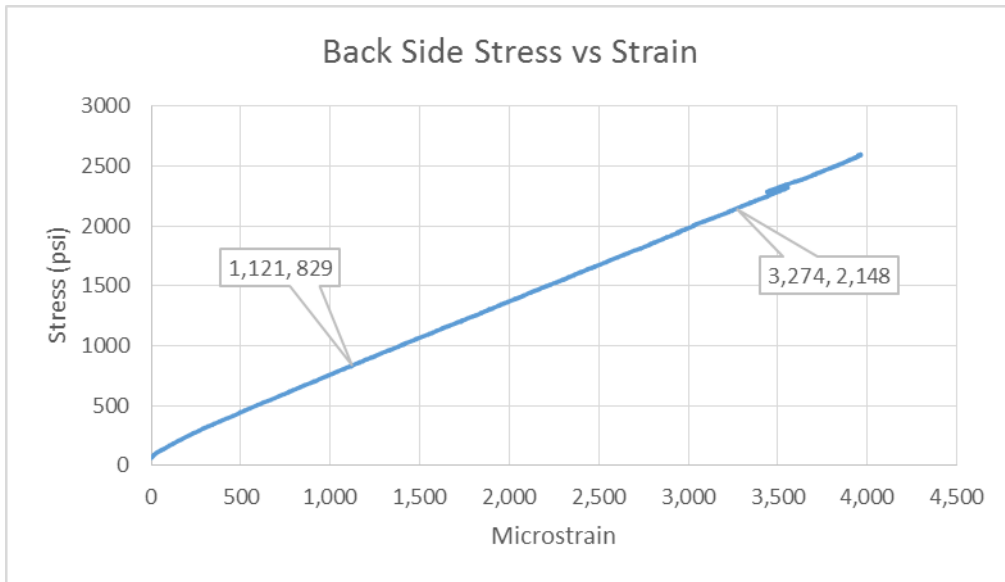


**Figure 27. 0.2A Back side test results**

**Specimen 0.3A**
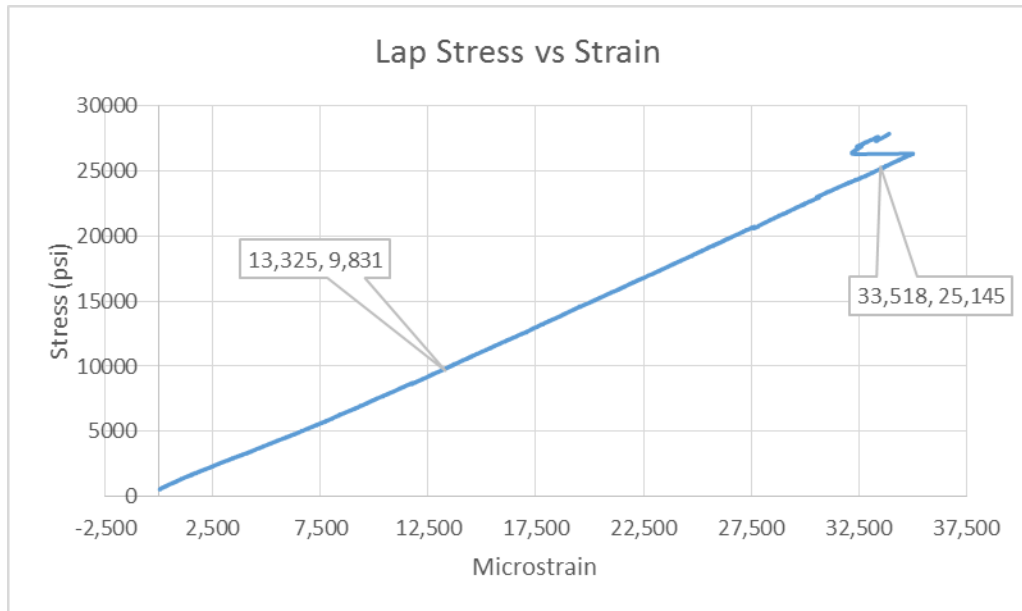


**Figure 28. 0.3A Lap test results**
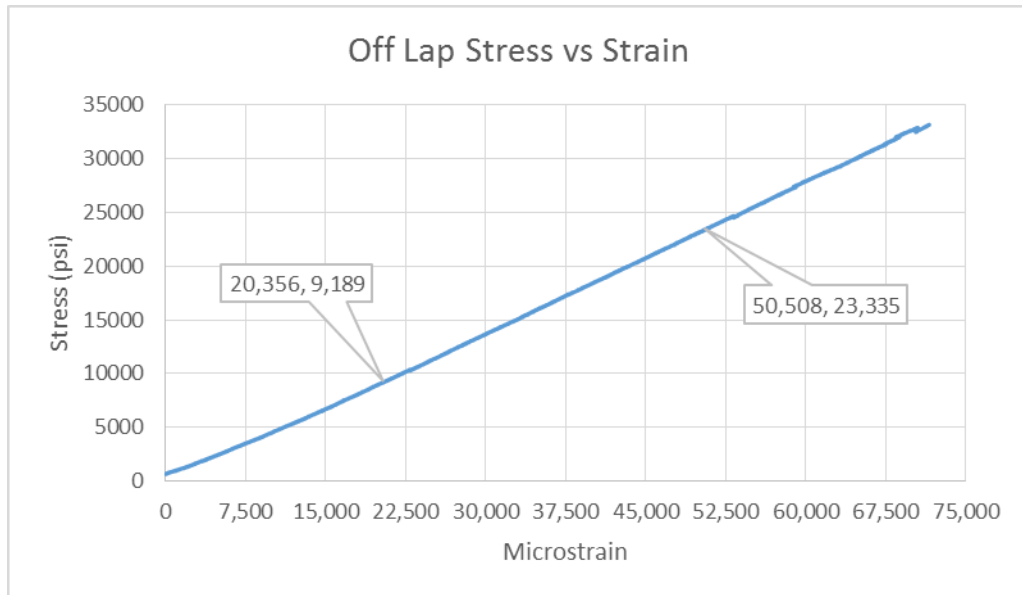


**Figure 29. 0.3A off lap test results**
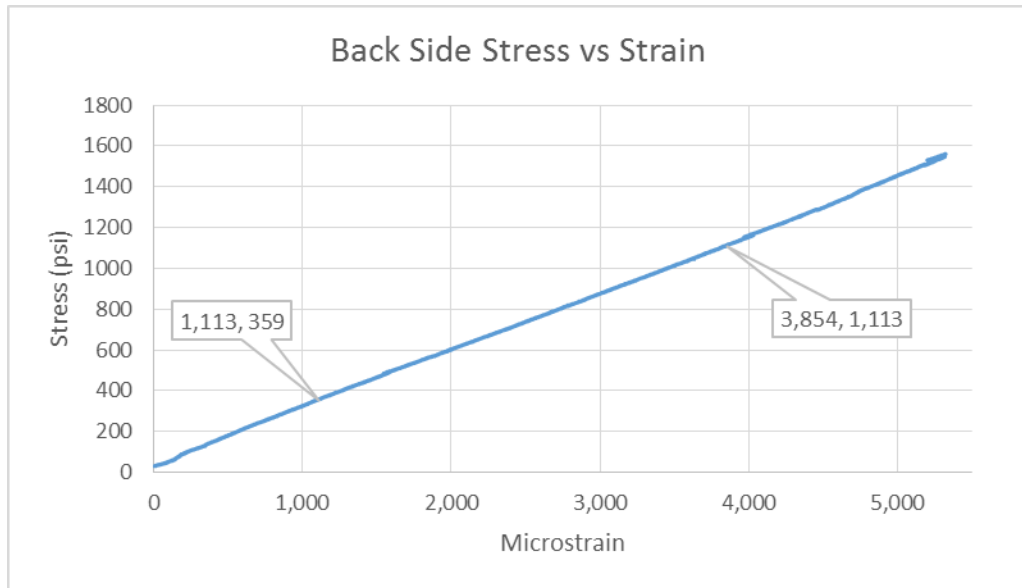
**Figure 30. 0.3A Back side test results**

**Specimen 0.4A**
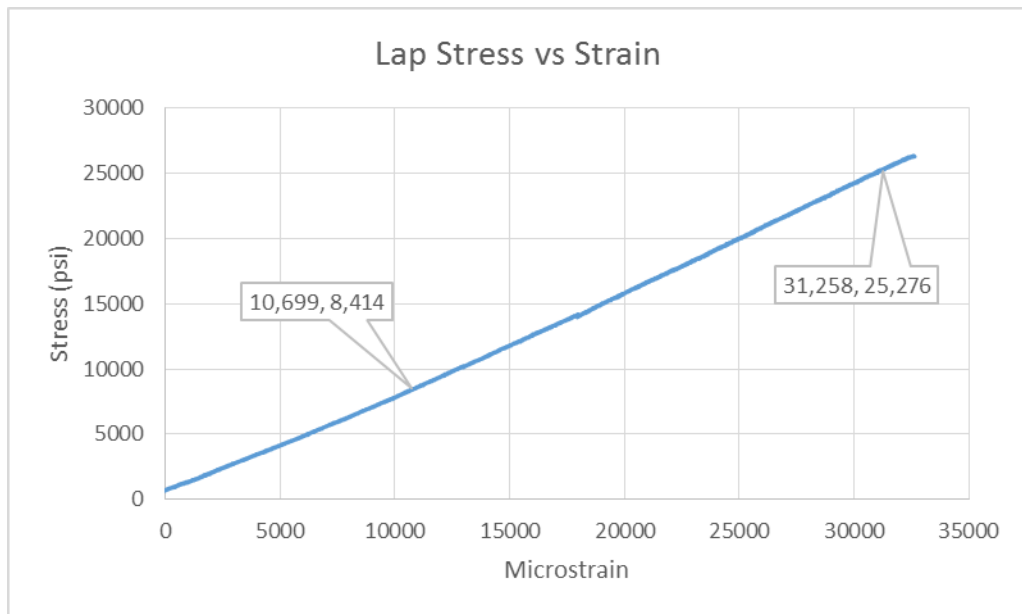


**Figure 31. 0.4A Lap results**
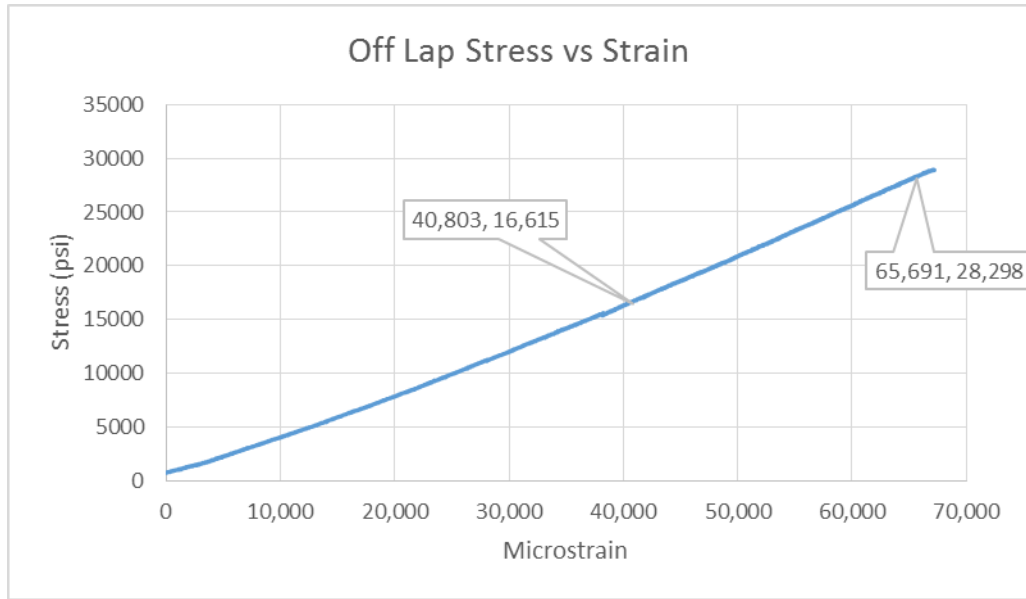
**Figure 32. 0.4A Off lap test results**
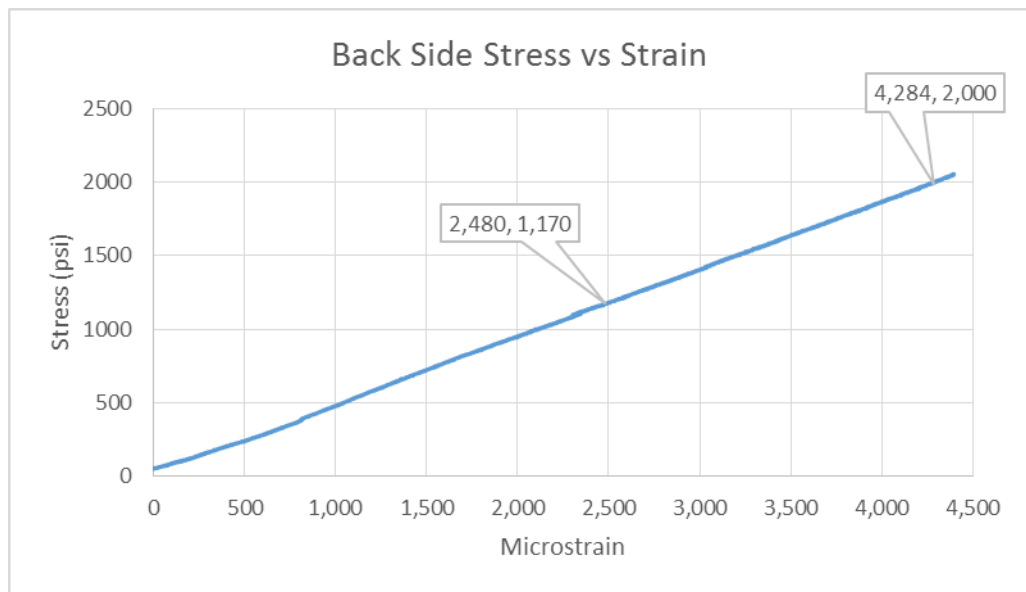


**Figure 33. 0.4A Back side test results**

**Specimen 1.3 test results**
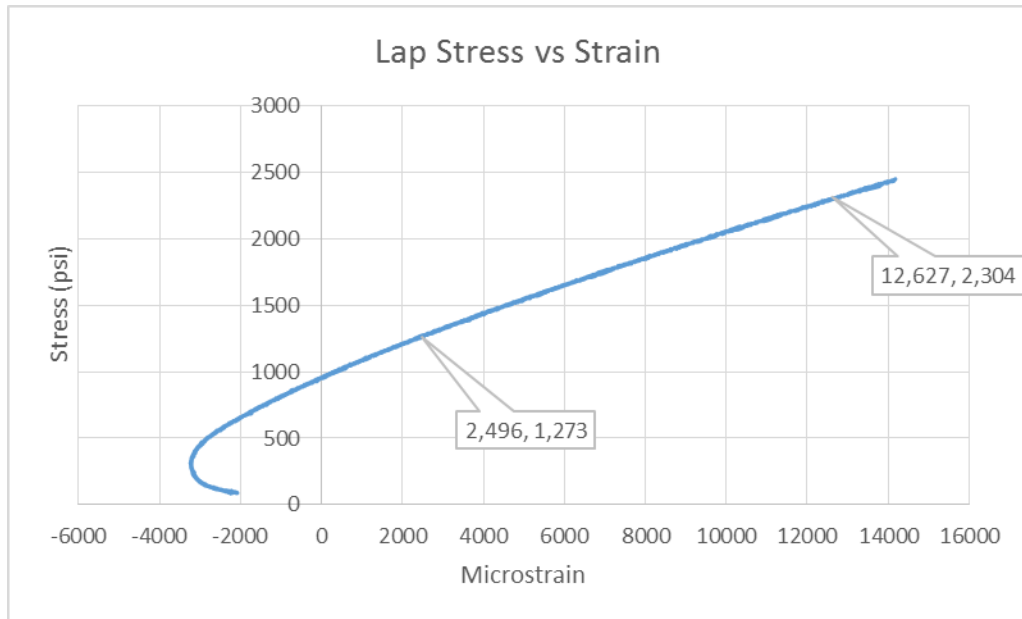


**Figure 34. 1.3 Lap test results**
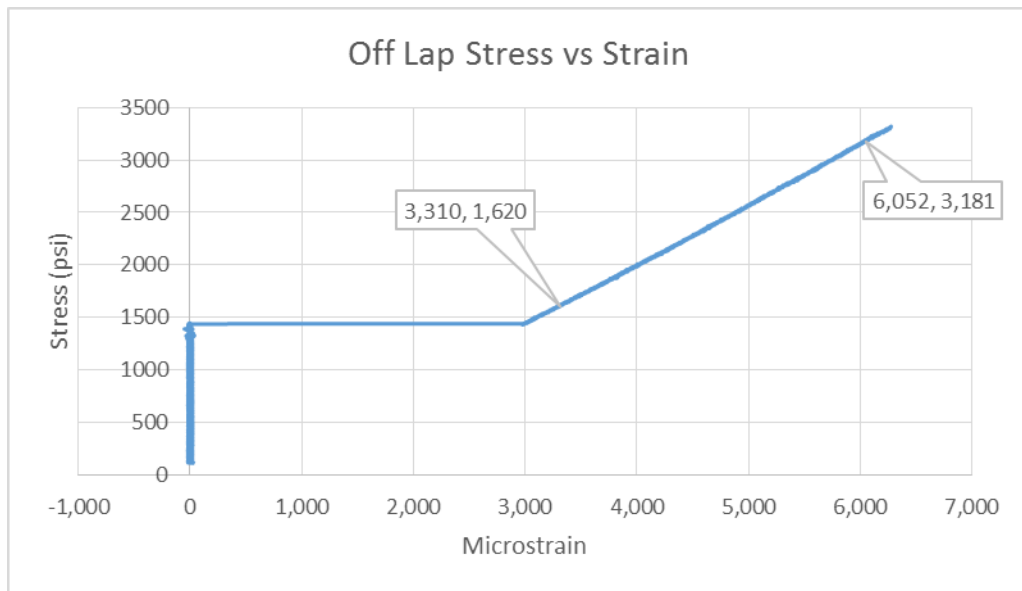


**Figure 35. 1.3 Off lap test results**
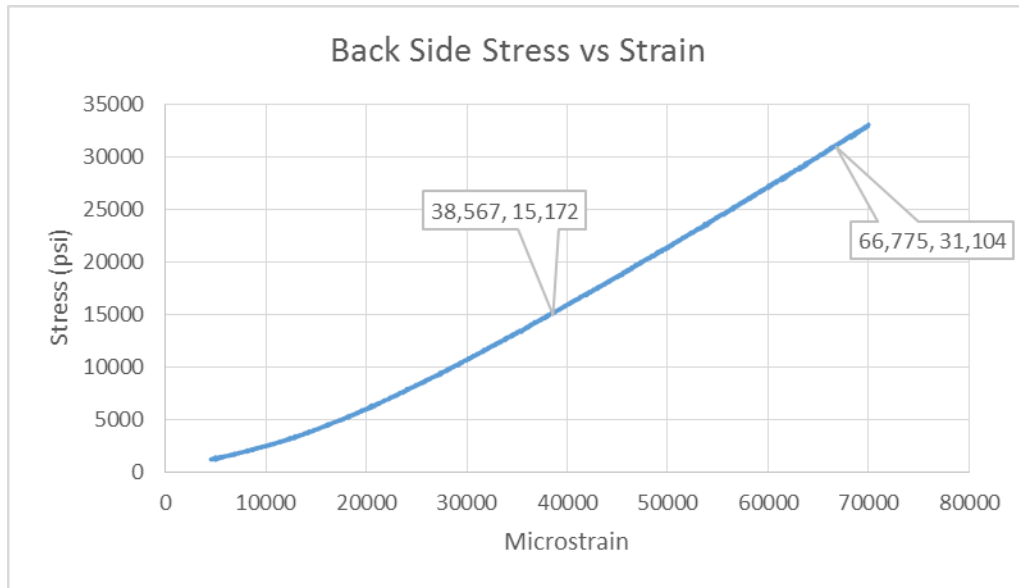
**Figure 36. 1.3 Back side test results**

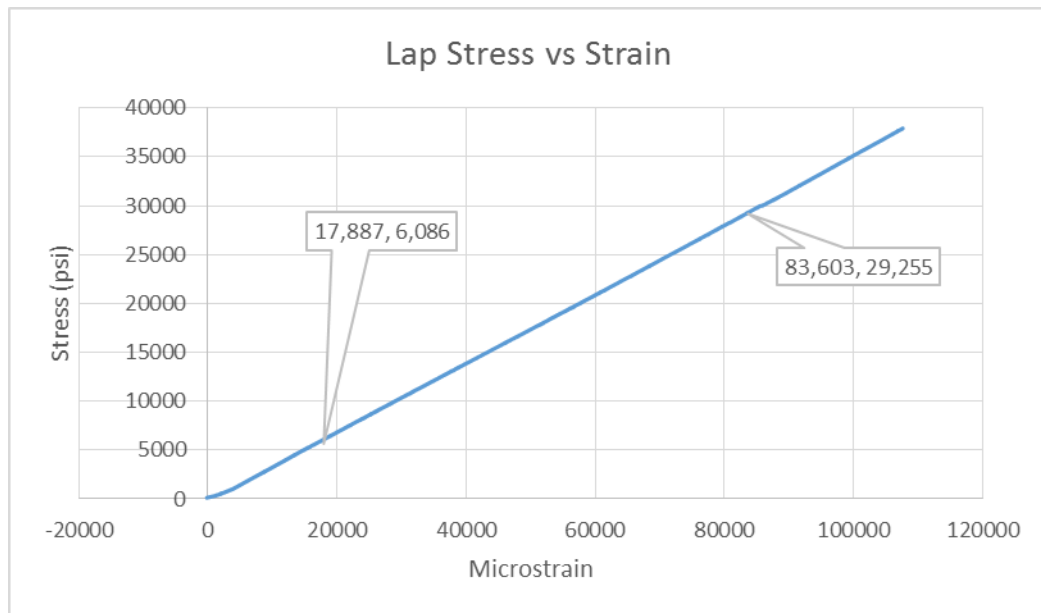**Specimen 1.4 test results**
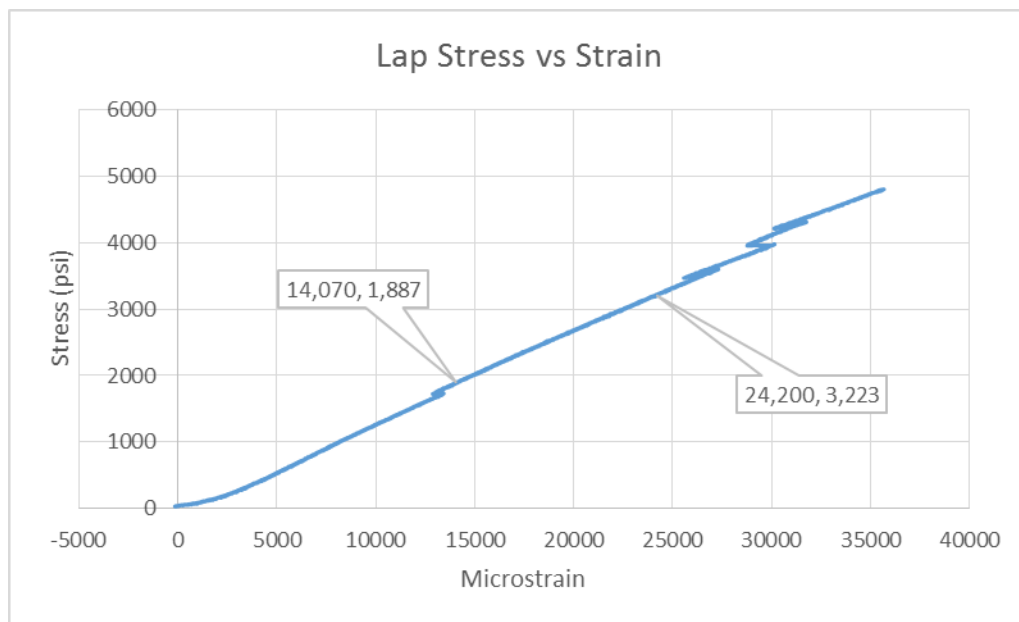


**Figure 37. 1.4 Lap test results**
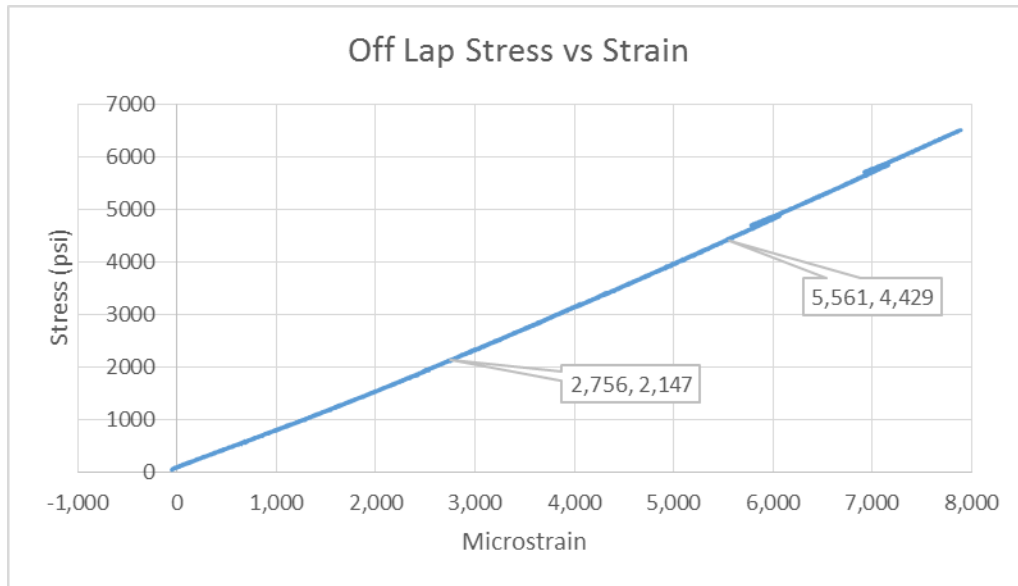
**Figure 38. 1.4 Off lap test results**
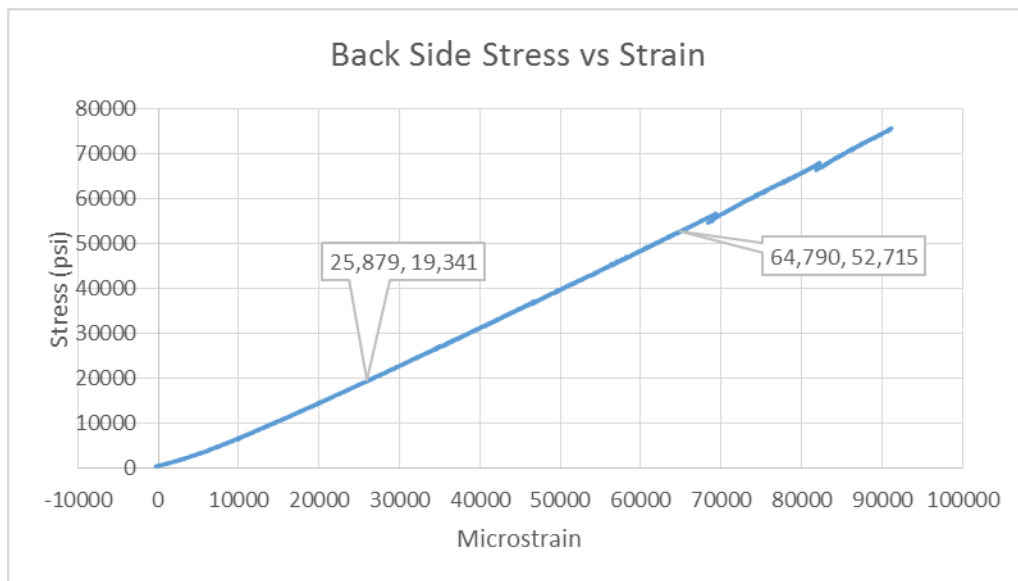


**Figure 39. 1.4 Back side test results**

**Specimen 1.5 test results**
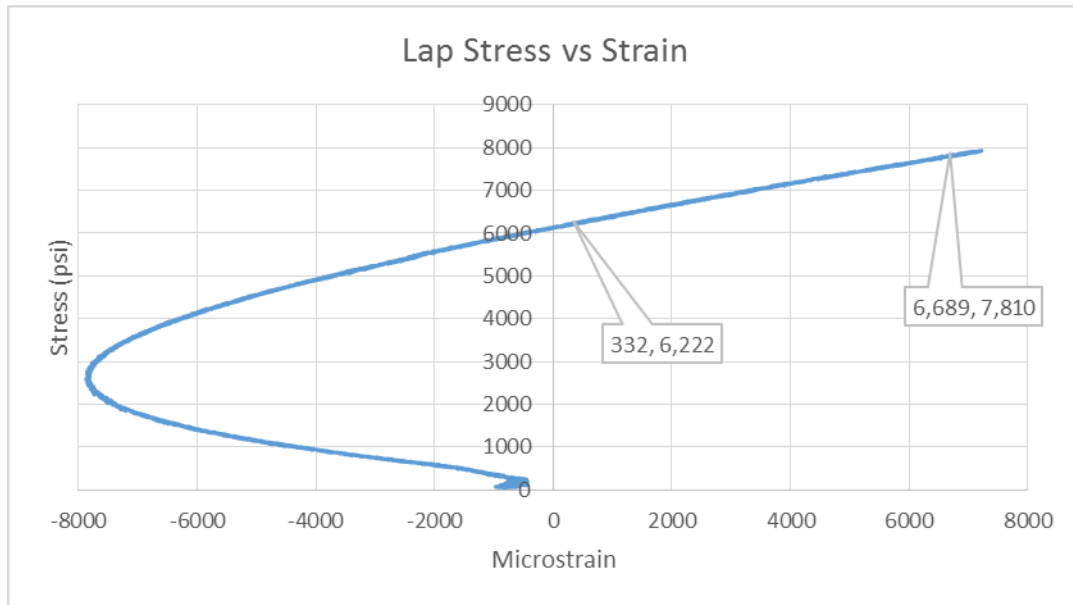


**Figure 40. 1.5 Lap test results**
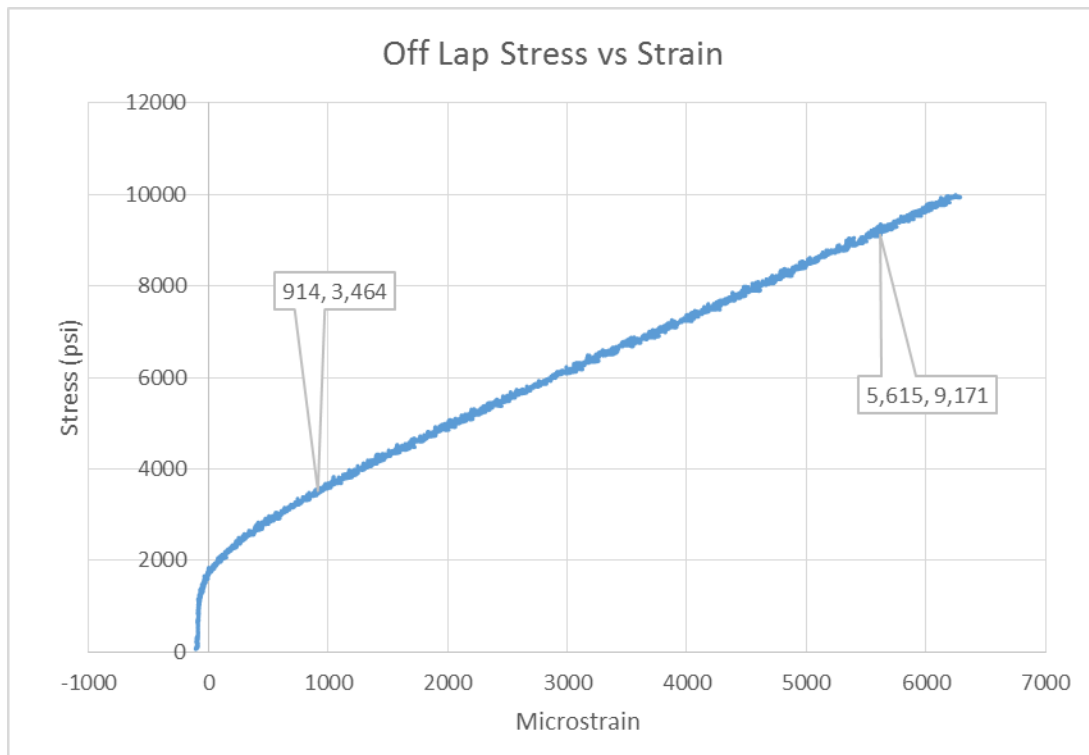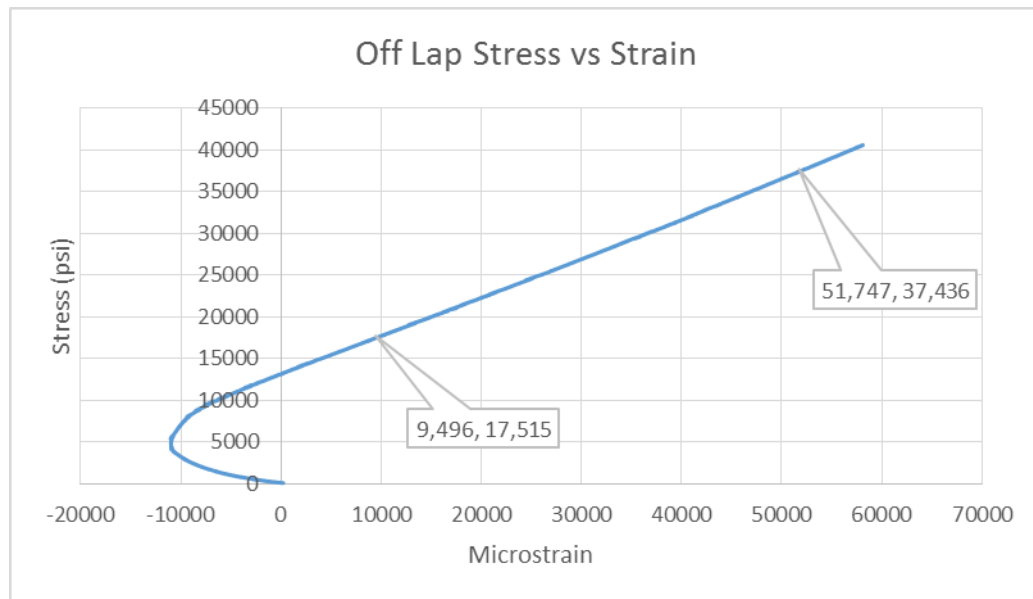


**Figure 41. 1.5 Off lap test results**
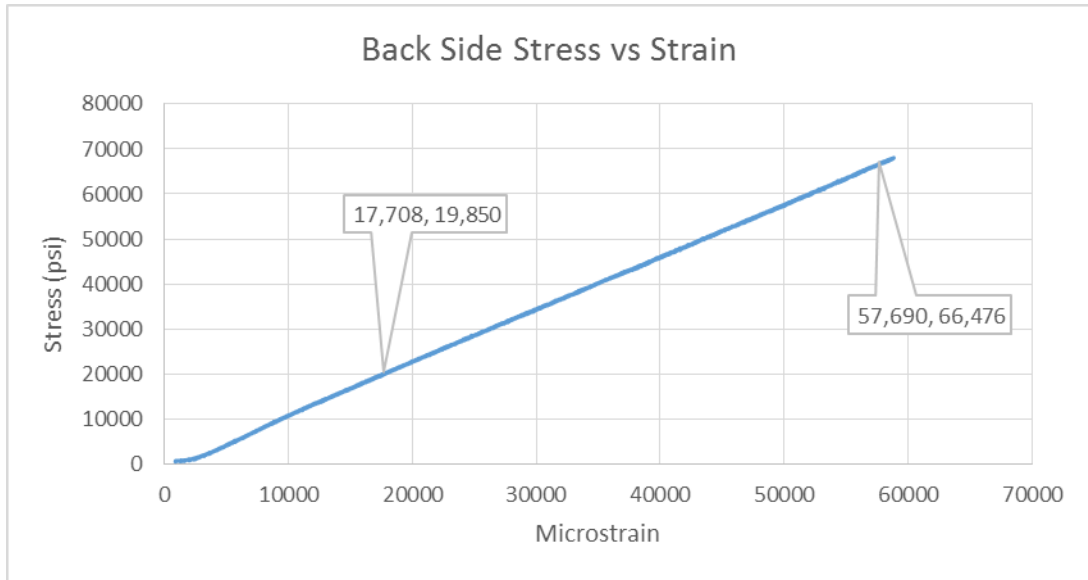
**Figure 42. 1.5 Back side test results**

**Specimen 1.6 test results**
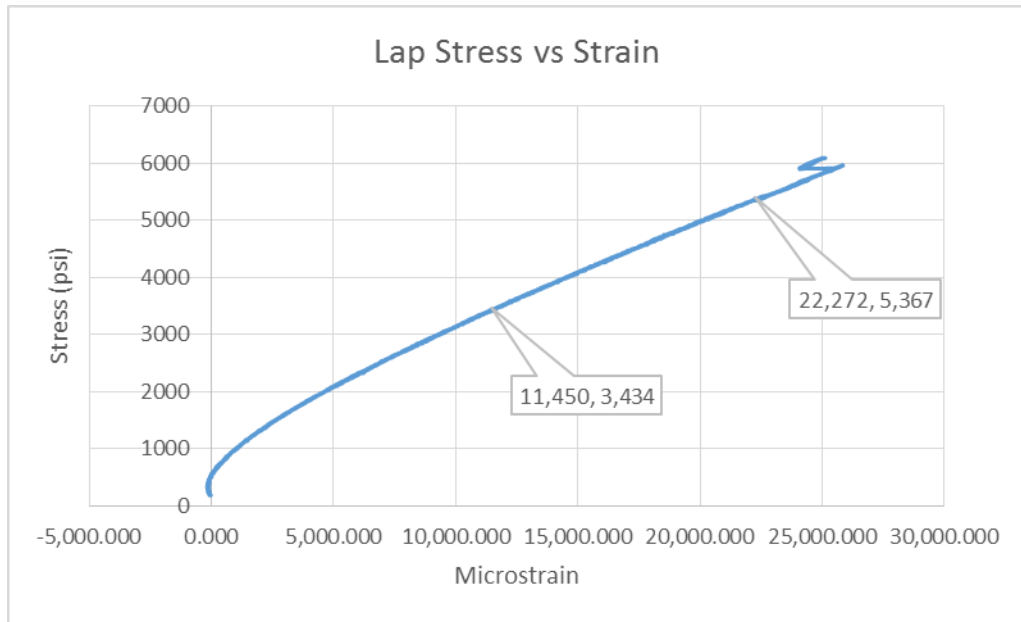


**Figure 43. 1.6 Lap test results**
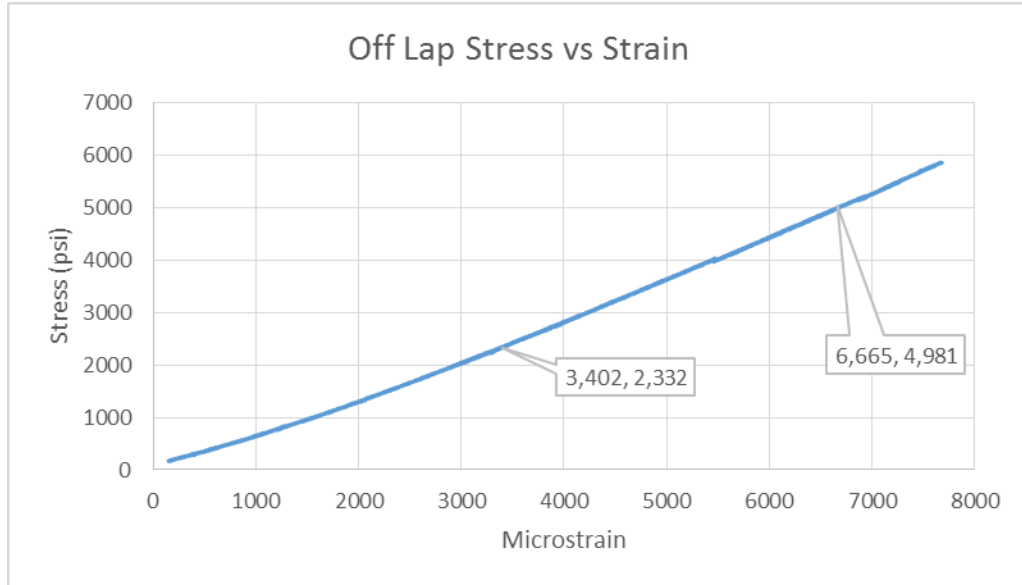
**Figure 44. 1.6 Off lap test results**
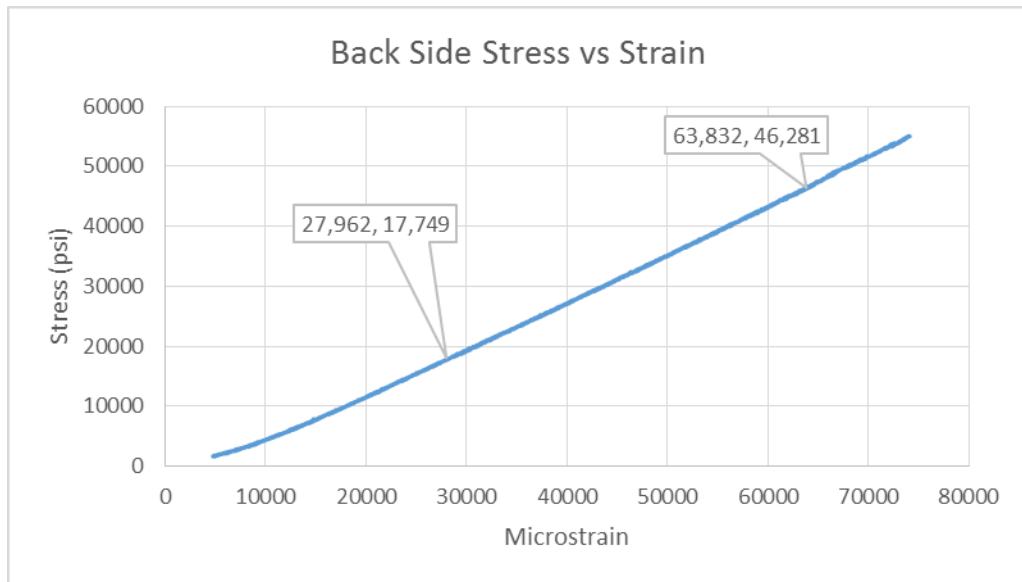


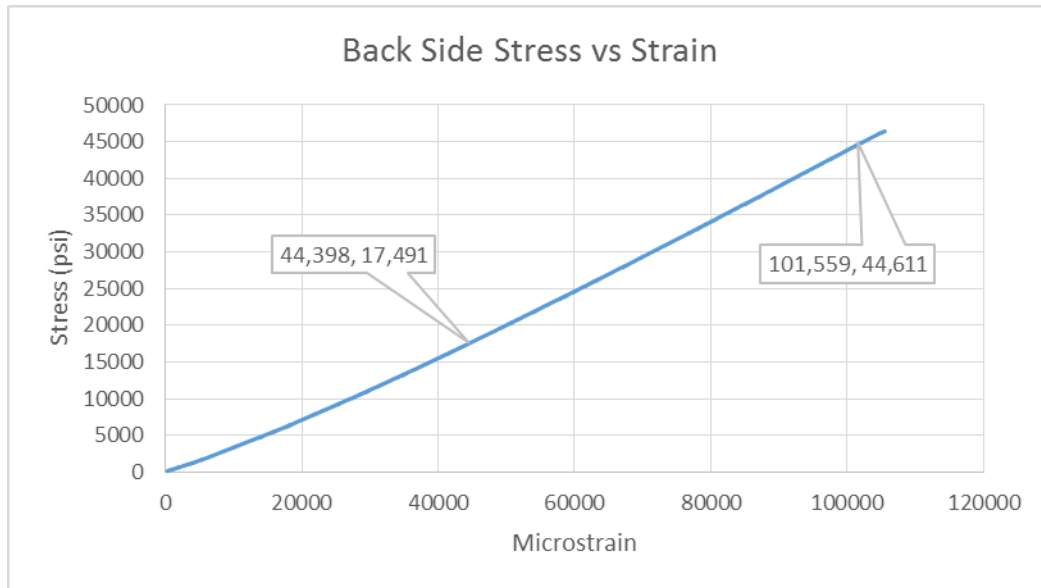**Figure 45. 1.6 Back side test results**

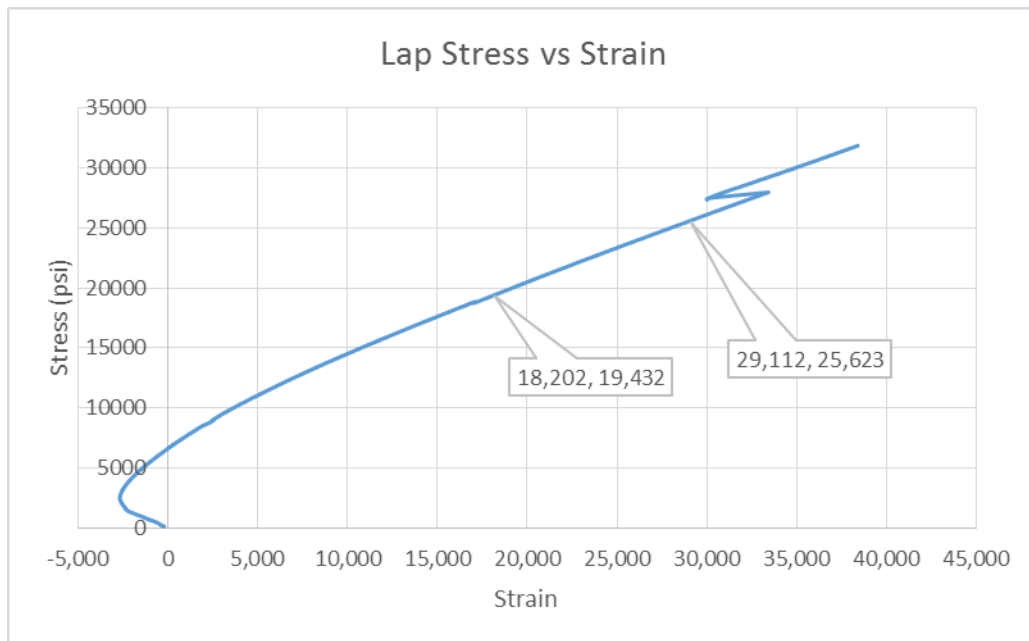**Specimen 2.1 test results**



**Figure 46. 2.1 Lap test results**
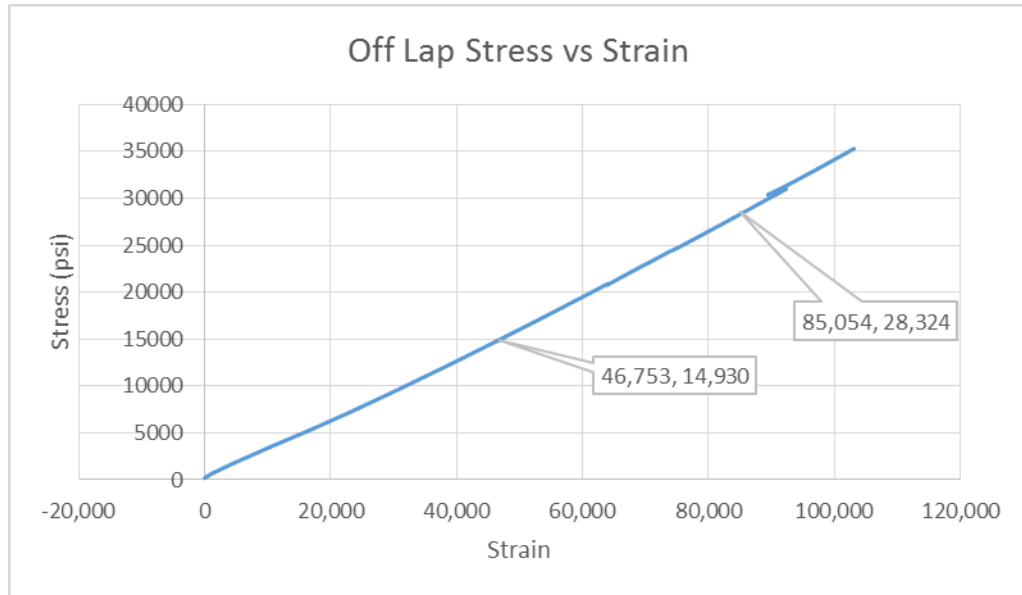


**Figure 47. 2.1 Off lap test results**
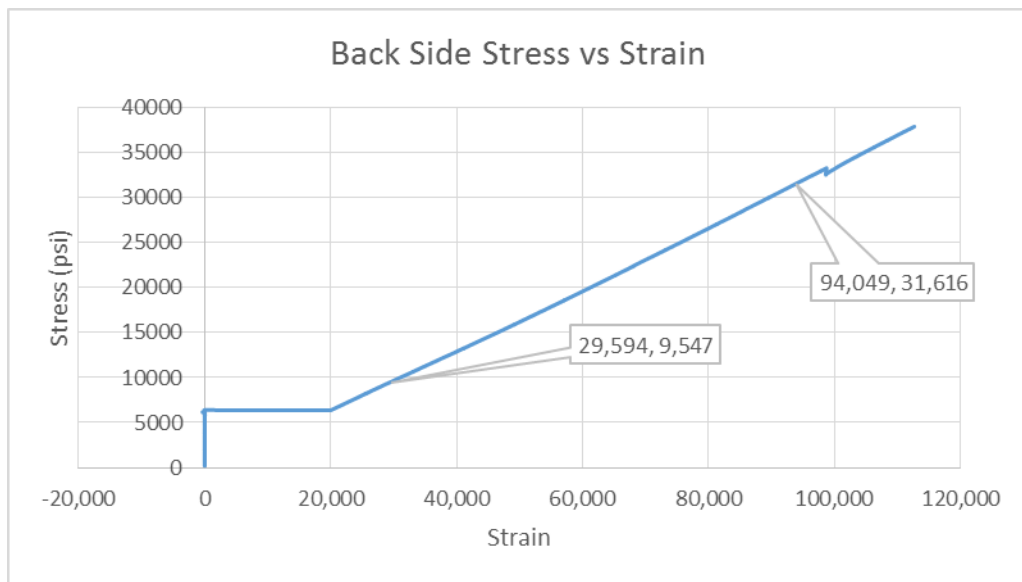
**Figure 48. 2.1 Back side test results**

**Specimen 2.2 test results**



**Figure 49. 2.2 Lap test results**

**Figure 50. 2.2 Off lap test results**



**Figure 51. 2.2 Back side test results**

**Specimen 2.3 test results**
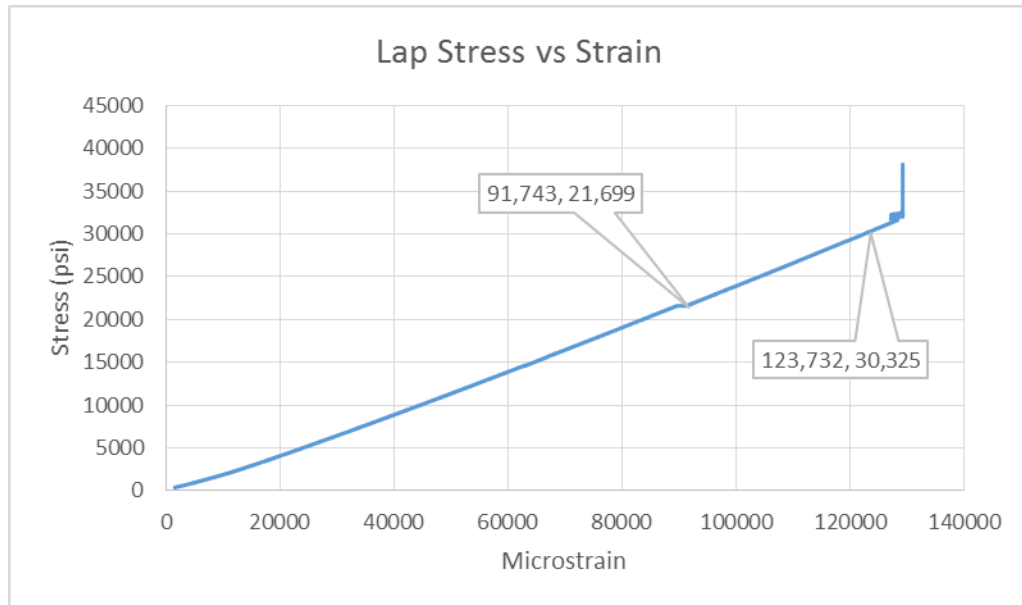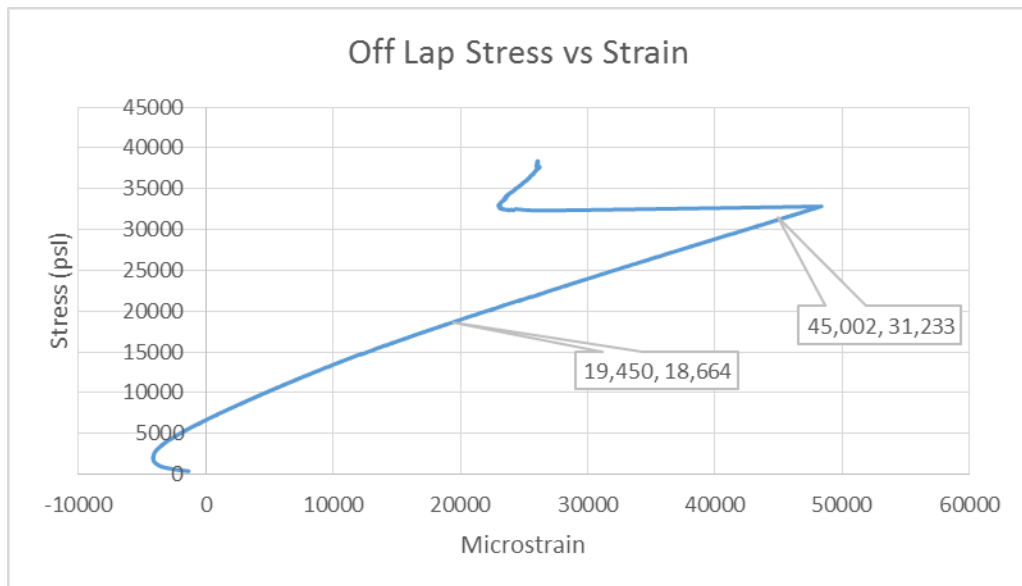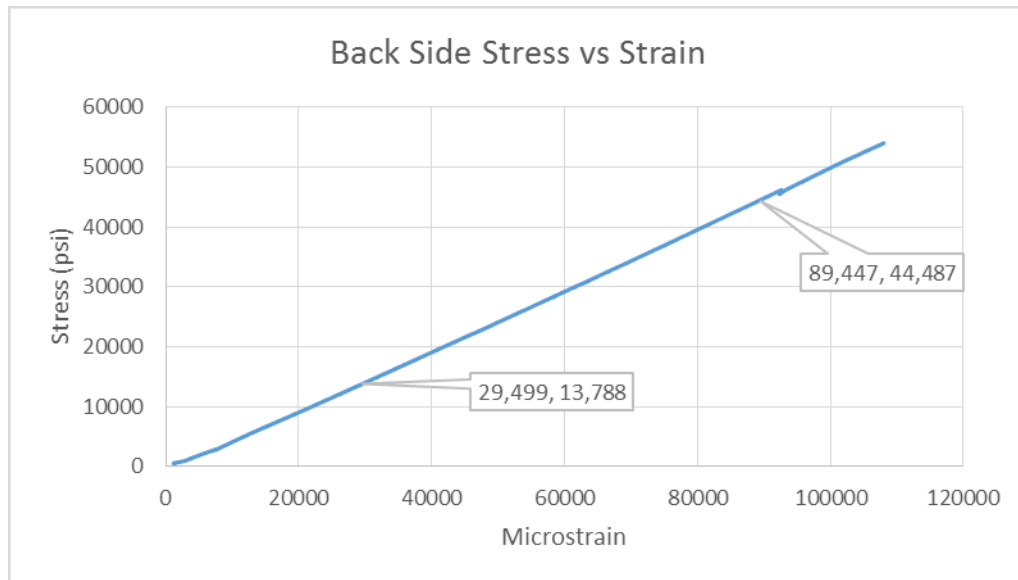


**Figure 52. 2.3 Lap test results**



**Figure 53. 2.3 Off lap test results**

**Figure 54. 2.3 Back side test results**

# Appendix B - Modified Volkersen Model Results

The equations shown below were used to determine the shear stress distribution according to the modified Volkersen model for each specimen. The shear stress distribution was then used to determine the actual stiffness and average stiffness of the lap joint.

Volkersen 1-Dimensional Shear Lag model

Assumptions:
1. Constant bond and adherend thickness.
2. Uniform distribution of shear strain through the adhesive thickness.
3. Adhesive carries only out-of-plane stresses while adherends carry only in-plane stresses.
4. Linear elastic material behavior.
5. Deformation of the adherends in the out-of-plane direction is negligible.

$$\tau(x) = \lambda\left[\left(\frac{P_x}{n} - \frac{C_0}{\lambda^2}\right)\frac{\sinh(\lambda x)}{\cosh(\lambda c)} + \frac{P_x}{n}\left(\frac{\cosh(\lambda x)}{\sinh(\lambda c)}\right)\right]$$

$$\lambda^2 = \frac{G_a}{t_a}\left(\frac{1}{E_o t_o} + \frac{1}{E_i(n-1)t_i}\right)$$

$$C_0 = \frac{G_a P_x}{E_i \times (n-1)t_i \times t_a}$$

$$G_a = \frac{E_a}{2(1 + v_m)}$$

Overlap length = 2c
$P_x$ = Applied force
$E_o$ = Modulus of elasticity of outer adherend, ksi
$E_i$ = Modulus of elasticity of inner adherend, ksi
$t_o$ = thickness of outer adherend, in.
$t_i$ = thickness of inner adherend, in.
$t_a$ = thcikness of adhesive, in.
$G_a$ = Shear modulus of adhesive, ksi
$n$ = Total number of layers at lap

**Figure 55. Equations used in modified Volkersen model**

**Specimen 0.2A**

| Specimen Properties: | | | | | | |
|---|---|---|---|---|---|---|
| $E_o =$ | 33,400.00 | ksi | | | | |
| $E_i =$ | 33,400.00 | ksi | $C_o =$ | | 987.9 | kip/in.$^3$ |
| $G_a =$ | 123.02 | ksi | $\lambda^2 =$ | | 61.07 | in.$^{-2}$ |
| $t_o =$ | 0.005045 | in. | $\lambda =$ | | 7.81 | in.$^{-1}$ |
| $t_i =$ | 0.005045 | in. | $C_o/\lambda^2 =$ | | 16.18 | kip/in |
| $t_a =$ | 0.023910 | in. | | | | |
| $P_x =$ | 32.353 | kip/in. | $P_x/n =$ | | 16.18 | kip/in. |
| $c = \pm$ | 3 | in. | | | | |
| $n =$ | 2 | | | | | |
| $E_a =$ | 419.00 | ksi | $C_o/\lambda =$ | | 126,412.68 | psi |
| $v_m =$ | 0.703 | | | | | |

**Figure 56. Properties to calculate specimen 0.2A stress distribution**
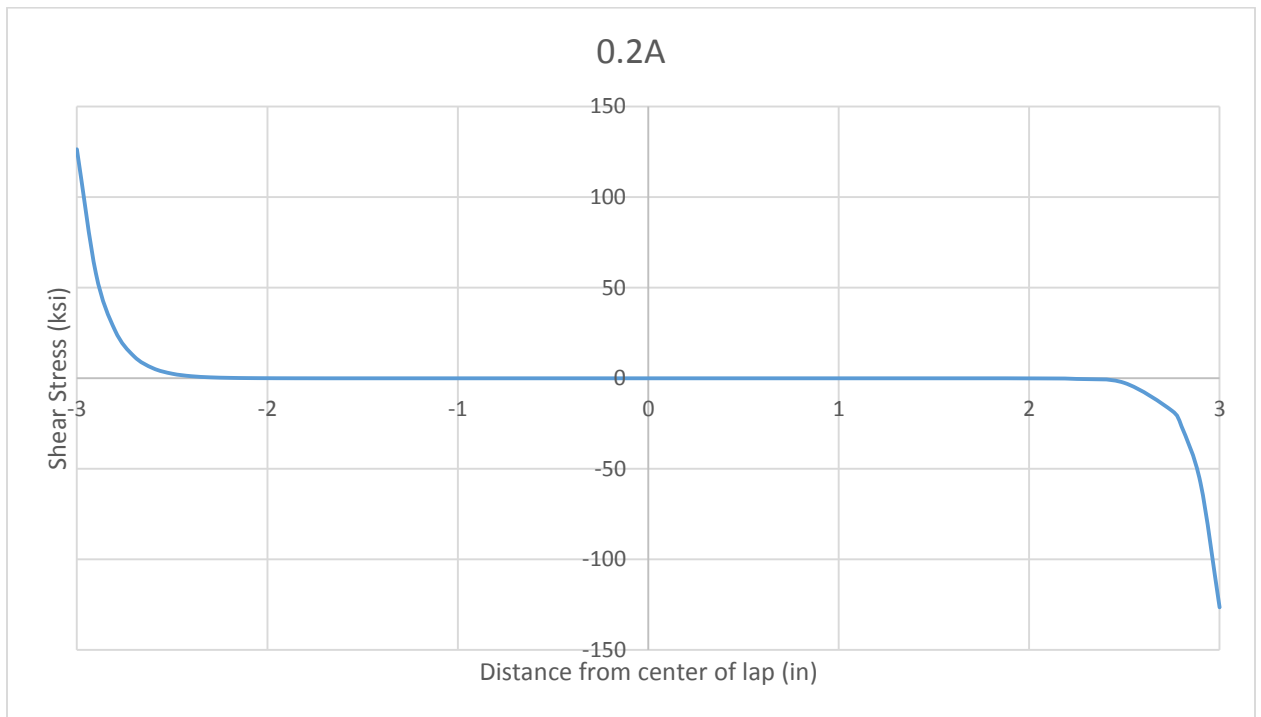


**Figure 57. 0.2A adhesive shear stress distribution**
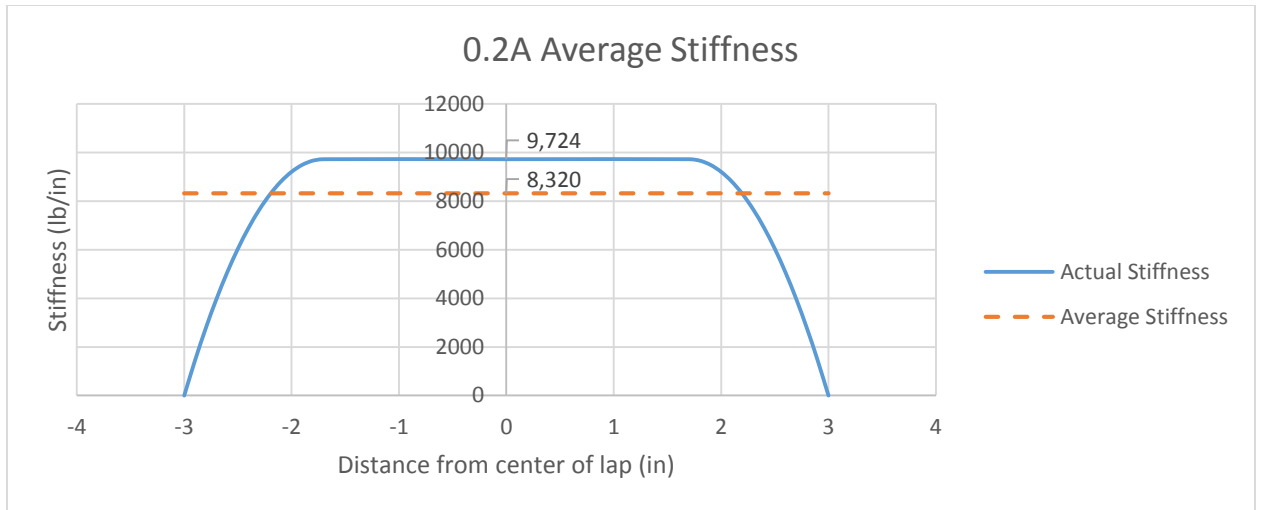
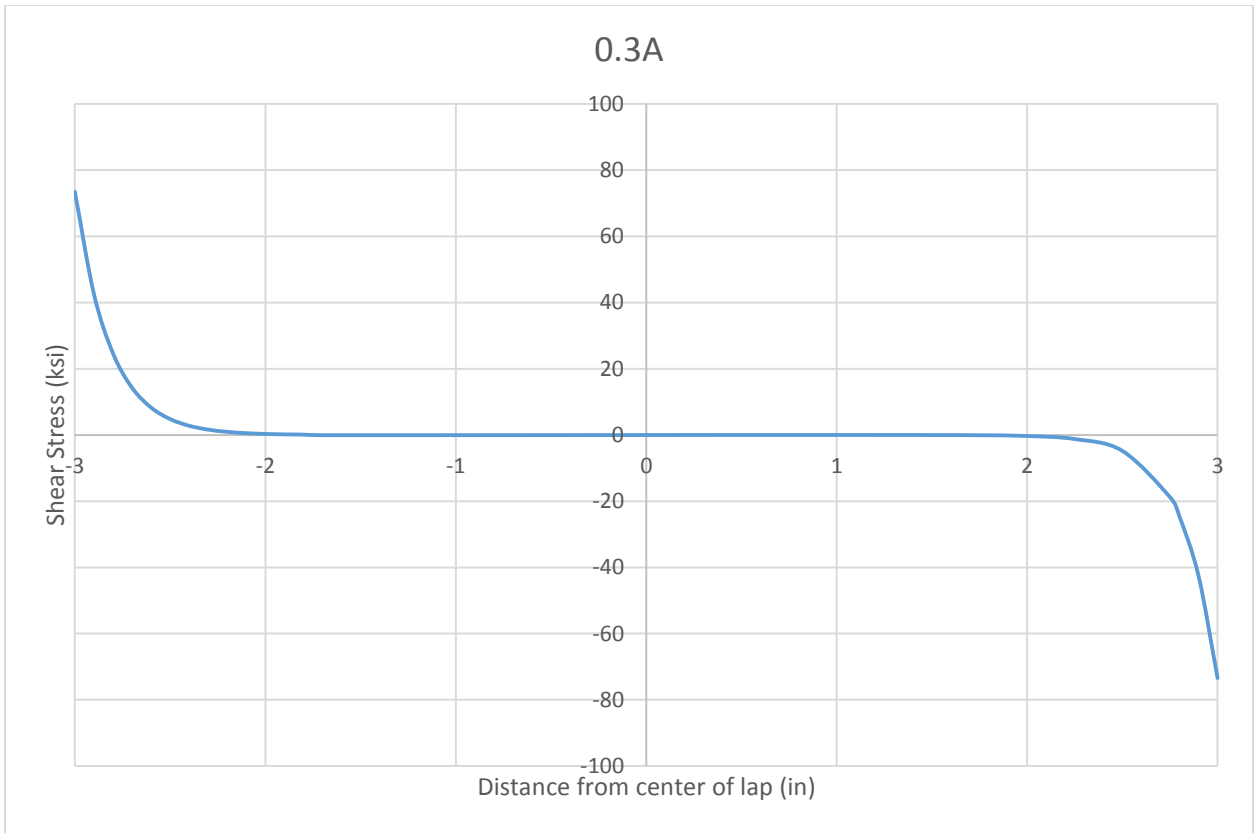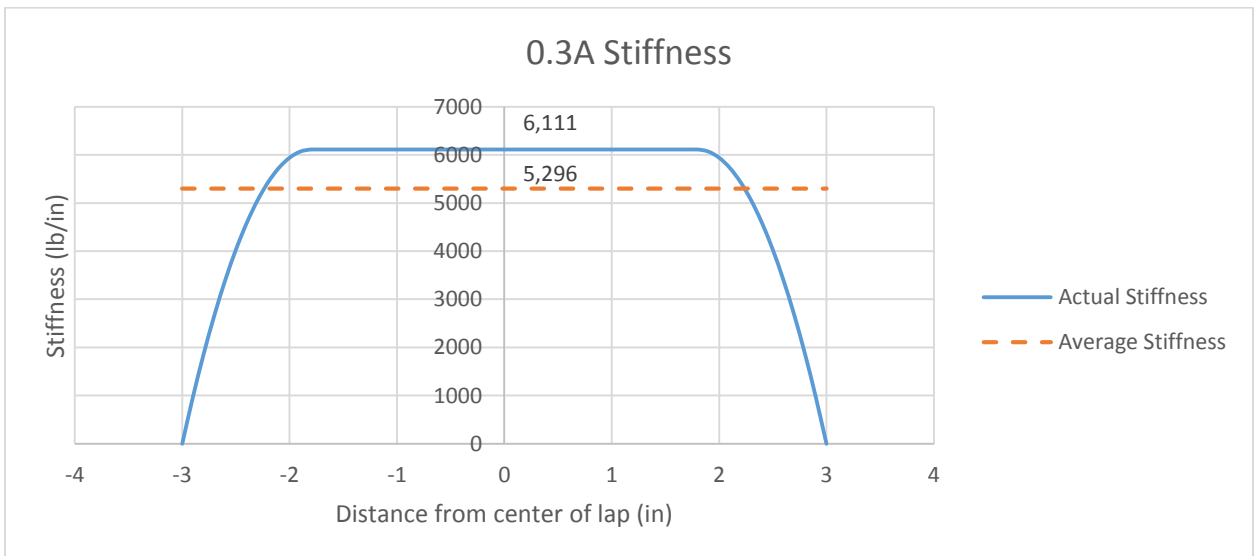**Figure 58. 0.2A joint stiffness**

## Specimen 0.3 A

| Specimen Properties: | | | | | | |
|---|---|---|---|---|---|---|
| $E_o =$ | 33,400.00 | ksi | | | | |
| $E_i =$ | 33,400.00 | ksi | $C_o =$ | 400.6 | kip/in.$^3$ | |
| $G_a =$ | **115.11** | ksi | $\lambda^2 =$ | 29.76 | in.$^{-2}$ | |
| $t_o =$ | 0.005045 | in. | $\lambda =$ | 5.46 | in.$^{-1}$ | |
| $t_i =$ | 0.005045 | in. | $C_o/\lambda^2 =$ | 13.46 | kip/in | |
| $t_a =$ | 0.045910 | in. | | | | |
| $P_x =$ | 26.923 | kip/in. | $P_x/n =$ | 13.46 | kip/in. | |
| $c = \pm$ | 3 | in. | | | | |
| $n =$ | 2 | | | | | |
| $E_a =$ | 419.00 | ksi | $C_o/\lambda =$ | 73,435.71 | psi | |
| $v_m =$ | 0.82 | | | | | |

**Figure 59. Properties to calculate specimen 0.3A stress distribution**
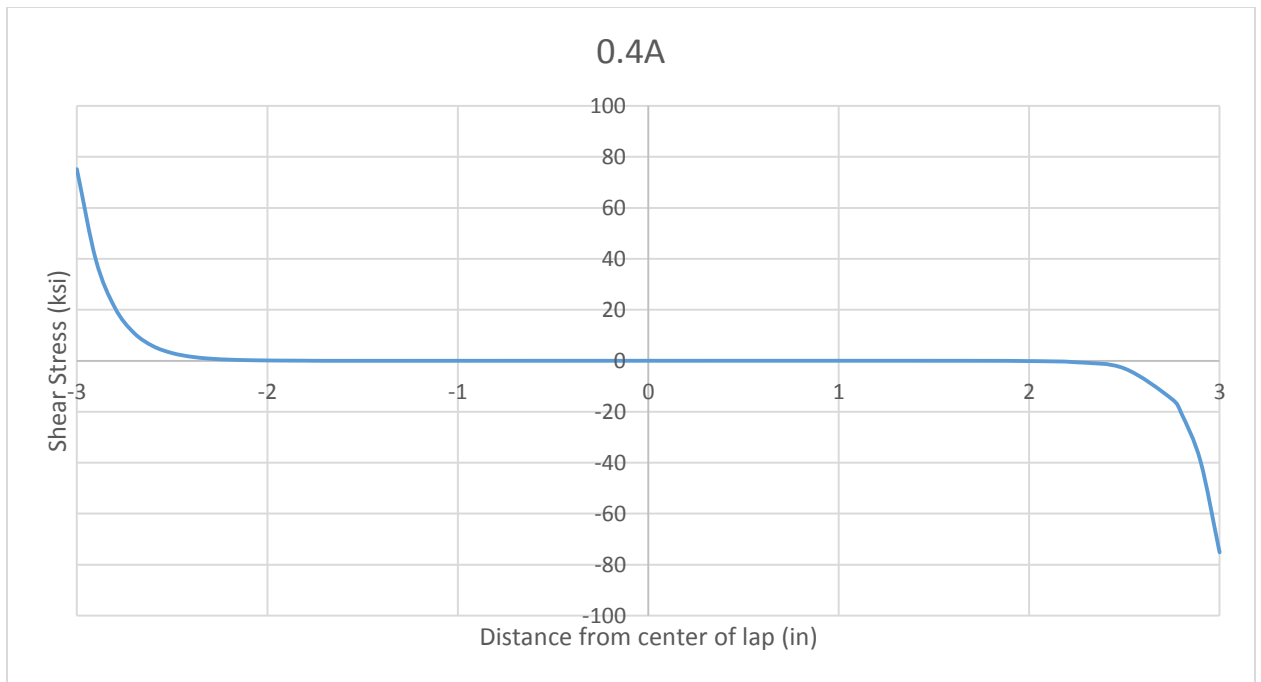
**Figure 60. 0.3A adhesive shear stress distribution**



**Figure 61. 0.3A joint stiffness**

**Specimen 0.4A**

| Specimen Properties: | | | | | | | |
|---|---|---|---|---|---|---|---|
| $E_o =$ | 33,400.00 | ksi | | | | | |
| $E_i =$ | 33,400.00 | ksi | $C_o =$ | 483.6 | kip/in.$^3$ | | |
| $G_a =$ | 118.29 | ksi | $\lambda^2 =$ | 41.41 | in.$^{-2}$ | | |
| $t_o =$ | 0.005045 | in. | $\lambda =$ | 6.43 | in.$^{-1}$ | | |
| $t_i =$ | 0.005045 | in. | $C_o/\lambda^2 =$ | 11.68 | kip/in | | |
| $t_a =$ | 0.033910 | in. | | | | | |
| $P_x =$ | 23.358 | kip/in. | $P_x/n =$ | 11.68 | kip/in. | | |
| $c = \pm$ | 3 | in. | | | | | |
| $n =$ | 2 | | | | | | |
| $E_a =$ | 419.00 | ksi | $C_o/\lambda =$ | 75,151.16 | psi | | |
| $v_m =$ | 0.771 | | | | | | |

**Figure 62. Properties to calculate specimen 0.4A stress distribution**



**Figure 63. 0.4A adhesive shear stress distribution**

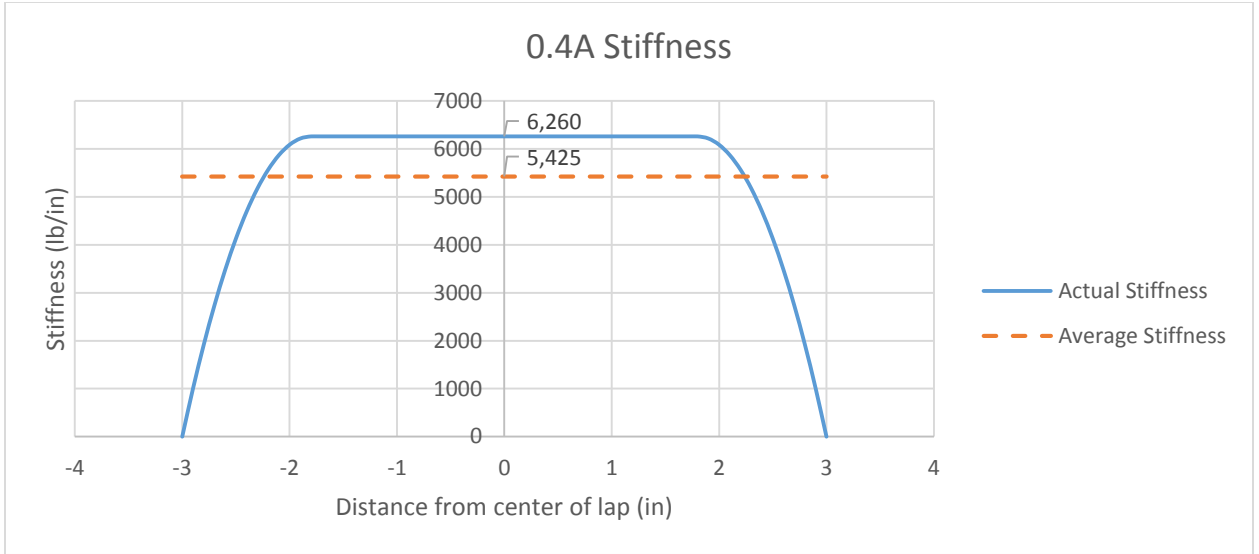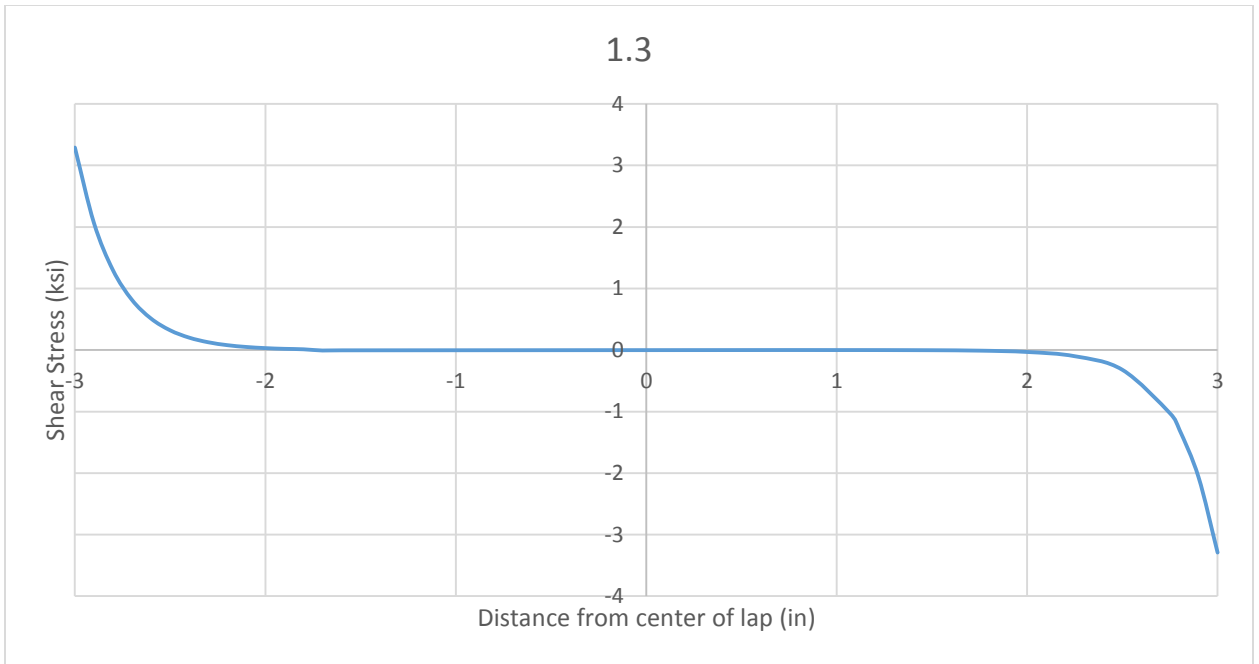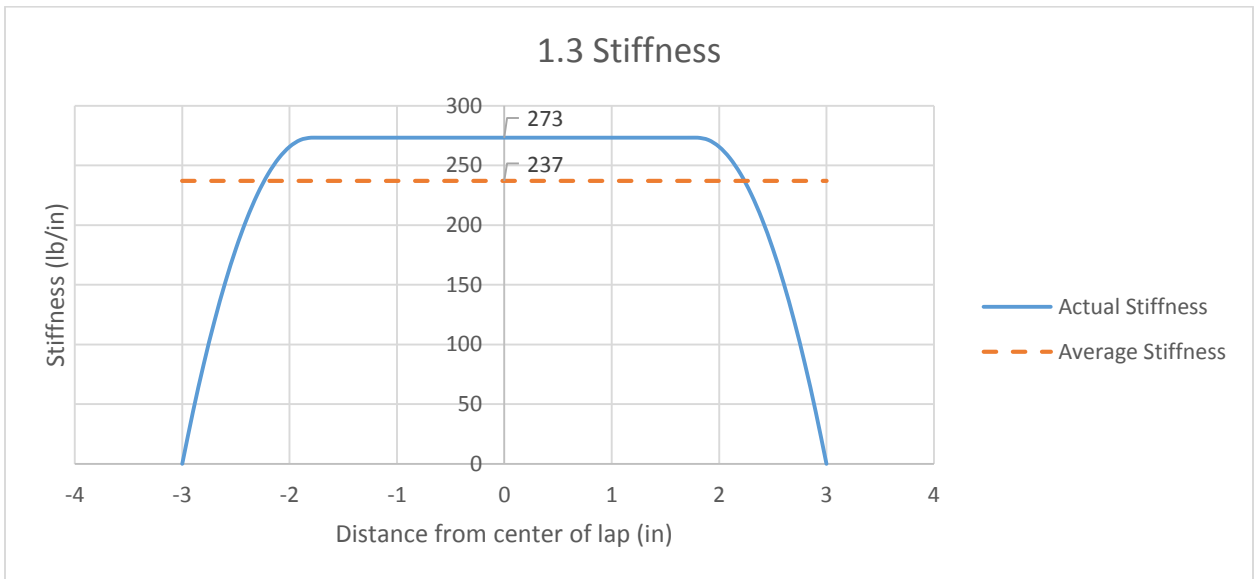**Figure 64. 0.4A joint stiffness**

**Specimen 1.3**

| Specimen Properties: | | | | | | |
|---|---|---|---|---|---|---|
| $E_o =$ | 33,400.00 | ksi | | | | |
| $E_i =$ | 33,400.00 | ksi | $C_o =$ | 15.3 | kip/in.$^3$ | |
| $G_a =$ | 113.06 | ksi | $\lambda^2 =$ | 21.67 | in.$^{-2}$ | |
| $t_o =$ | 0.005045 | in. | $\lambda =$ | 4.65 | in.$^{-1}$ | |
| $t_i =$ | 0.005045 | in. | $C_o/\lambda^2 =$ | 0.71 | kip/in | |
| $t_a =$ | 0.046455 | in. | | | | |
| $P_x =$ | 2.121 | kip/in. | $P_x/n =$ | 0.71 | kip/in. | |
| $c = \pm$ | 3 | in. | | | | |
| $n =$ | 3 | | | | | |
| $E_a =$ | 419.00 | ksi | $C_o/\lambda =$ | 3,290.78 | psi | |
| $v_m =$ | 0.853 | | | | | |

**Figure 65. Properties to calculate specimen 1.3 stress distribution**
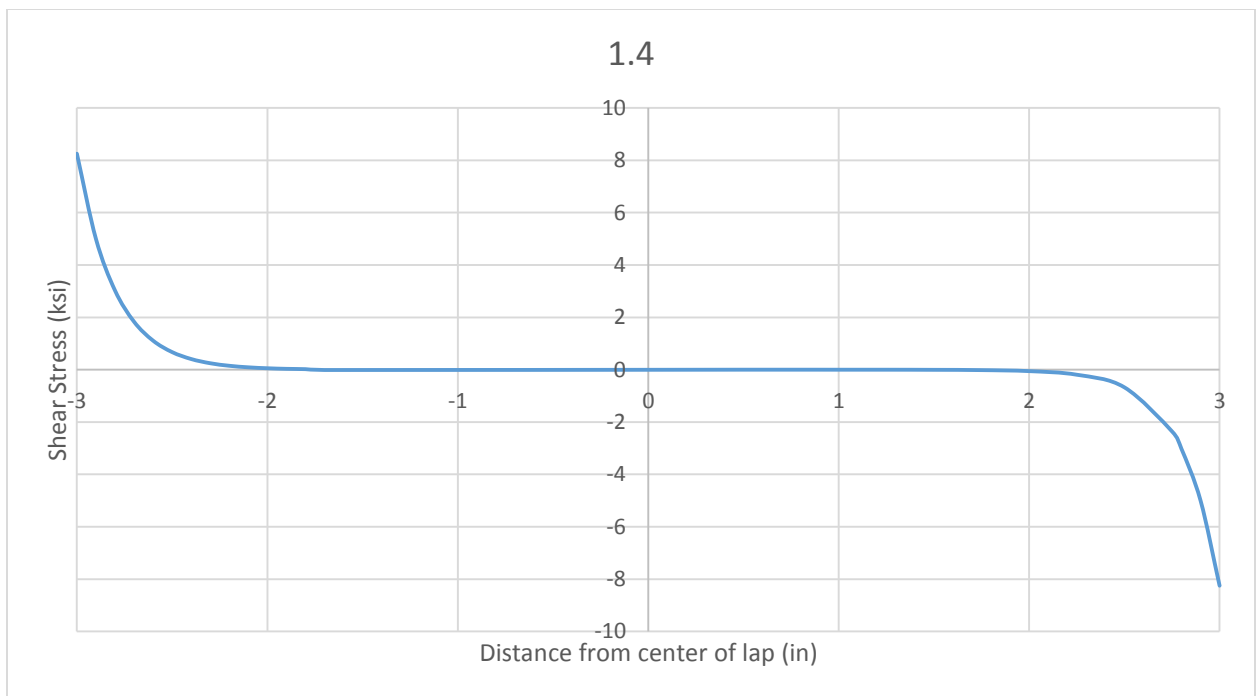
**Figure 66. 1.3 adhesive shear stress distribution**
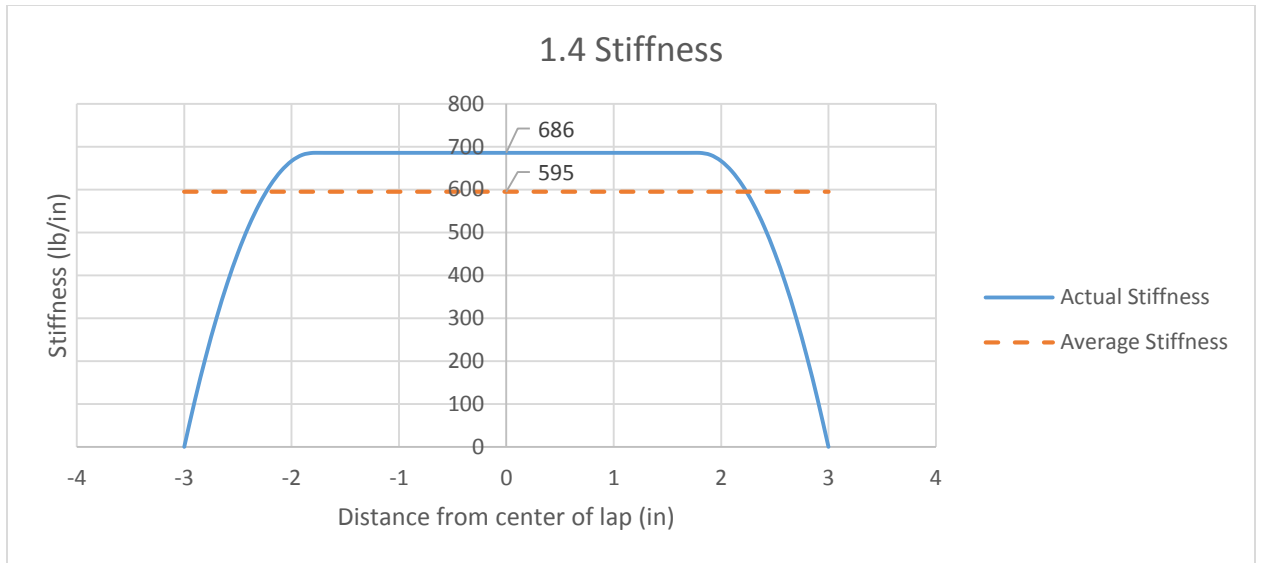


**Figure 67. 1.3 joint stiffness**

**Specimen 1.4**

| Specimen Properties: | | | | | | |
|---|---|---|---|---|---|---|
| $E_o =$ | 33,400.00 | ksi | | | | |
| $E_i =$ | 33,400.00 | ksi | $C_o =$ | | 41.4 | kip/in.$^3$ |
| $G_a =$ | 114.23 | ksi | $\lambda^2 =$ | | 25.14 | in.$^{-2}$ |
| $t_o =$ | 0.005045 | in. | $\lambda =$ | | 5.01 | in.$^{-1}$ |
| $t_i =$ | 0.005045 | in. | $C_o/\lambda^2 =$ | | 1.65 | kip/in |
| $t_a =$ | 0.040455 | in. | | | | |
| $P_x =$ | 4.937 | kip/in. | $P_x/n =$ | | 1.65 | kip/in. |
| $c = \pm$ | 3 | in. | | | | |
| $n =$ | 3 | | | | | |
| $E_a =$ | 419.00 | ksi | $C_o/\lambda =$ | | 8,250.68 | psi |
| $v_m =$ | 0.834 | | | | | |

**Figure 68. Properties to calculate specimen 1.4 stress distribution**
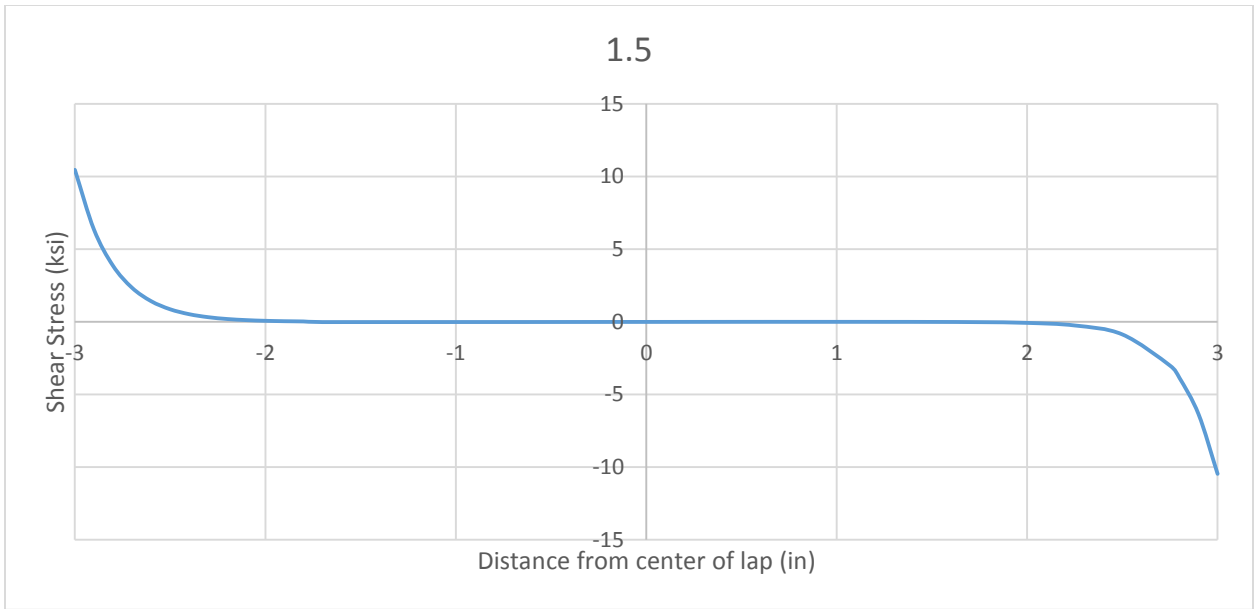


**Figure 69. 1.4 adhesive shear stress distribution**

65

**Figure 70. 1.4 joint stiffness**

## Specimen 1.5

| Specimen Properties: | | | | | | |
|---|---|---|---|---|---|---|
| $E_o$ = | 33,400.00 | ksi | | | | |
| $E_i$ = | 33,400.00 | ksi | $C_o$ = | 52.1 | kip/in.$^3$ | |
| $G_a$ = | 114.17 | ksi | $\lambda^2$ = | 24.82 | in.$^{-2}$ | |
| $t_o$ = | 0.005045 | in. | $\lambda$ = | 4.98 | in.$^{-1}$ | |
| $t_i$ = | 0.005045 | in. | $C_o/\lambda^2$ = | 2.10 | kip/in | |
| $t_a$ = | 0.040955 | in. | | | | |
| $P_x$ = | 6.3 | kip/in. | $P_x/n$ = | 2.10 | kip/in. | |
| c = ± | 3 | in. | | | | |
| n = | 3 | | | | | |
| $E_a$ = | 419.00 | ksi | $C_o/\lambda$ = | 10,461.20 | psi | |
| $v_m$ = | 0.835 | | | | | |

**Figure 71. Properties to calculate specimen 1.5 stress distribution**

**Figure 72. 1.5 adhesive shear stress distribution**
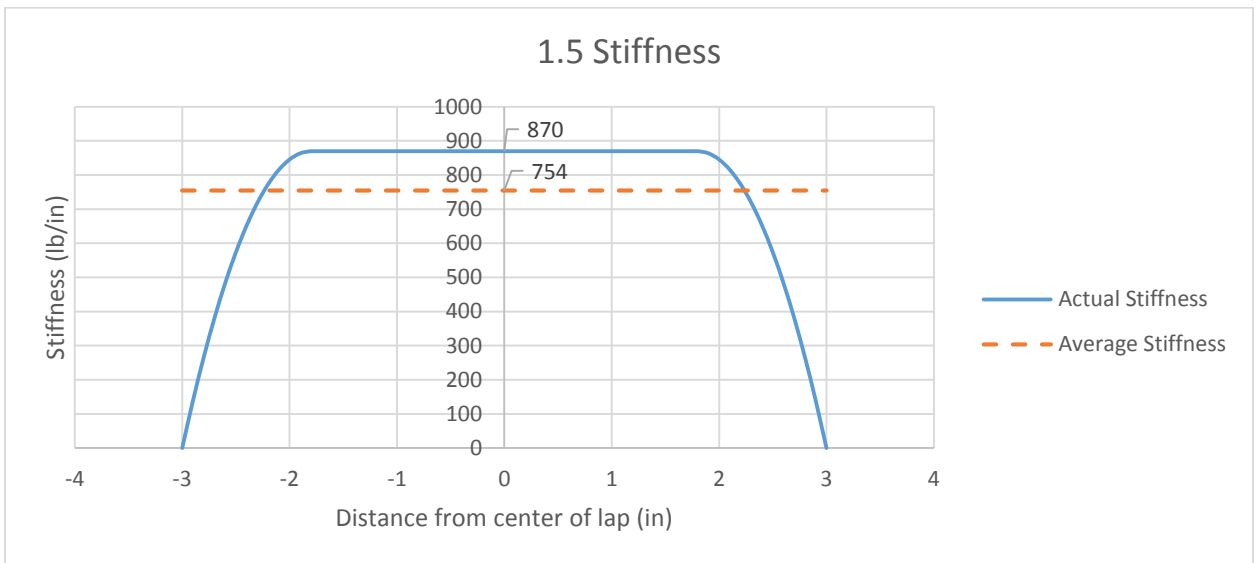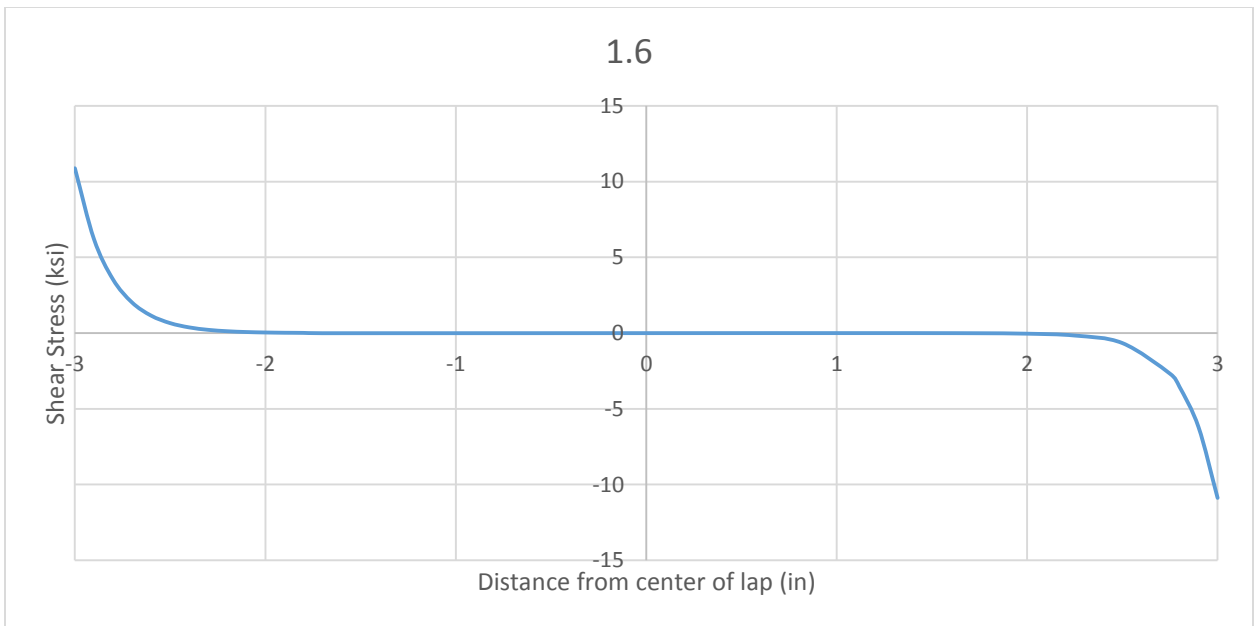


**Figure 73. 1.5 joint stiffness**

**Specimen 1.6**

| Specimen Properties: | | | | | | | |
|---|---|---|---|---|---|---|---|
| $E_o =$ | 33,400.00 | ksi | | | | | |
| $E_i =$ | 33,400.00 | ksi | $C_o =$ | | 61.0 | kip/in.$^3$ | |
| $G_a =$ | 116.32 | ksi | $\lambda^2 =$ | | 31.42 | in.$^{-2}$ | |
| $t_o =$ | 0.005045 | in. | $\lambda =$ | | 5.61 | in.$^{-1}$ | |
| $t_i =$ | 0.005045 | in. | $C_o/\lambda^2 =$ | | 1.94 | kip/in | |
| $t_a =$ | 0.032955 | in. | | | | | |
| $P_x =$ | 5.823 | kip/in. | $P_x/n =$ | | 1.94 | kip/in. | |
| $c = \pm$ | 3 | in. | | | | | |
| $n =$ | 3 | | | | | | |
| $E_a =$ | 419.00 | ksi | $C_o/\lambda =$ | | 10,880.32 | psi | |
| $v_m =$ | 0.801 | | | | | | |

**Figure 74. Properties to calculate specimen 1.6 stress distribution**



**Figure 75. 1.6 adhesive shear stress distribution**
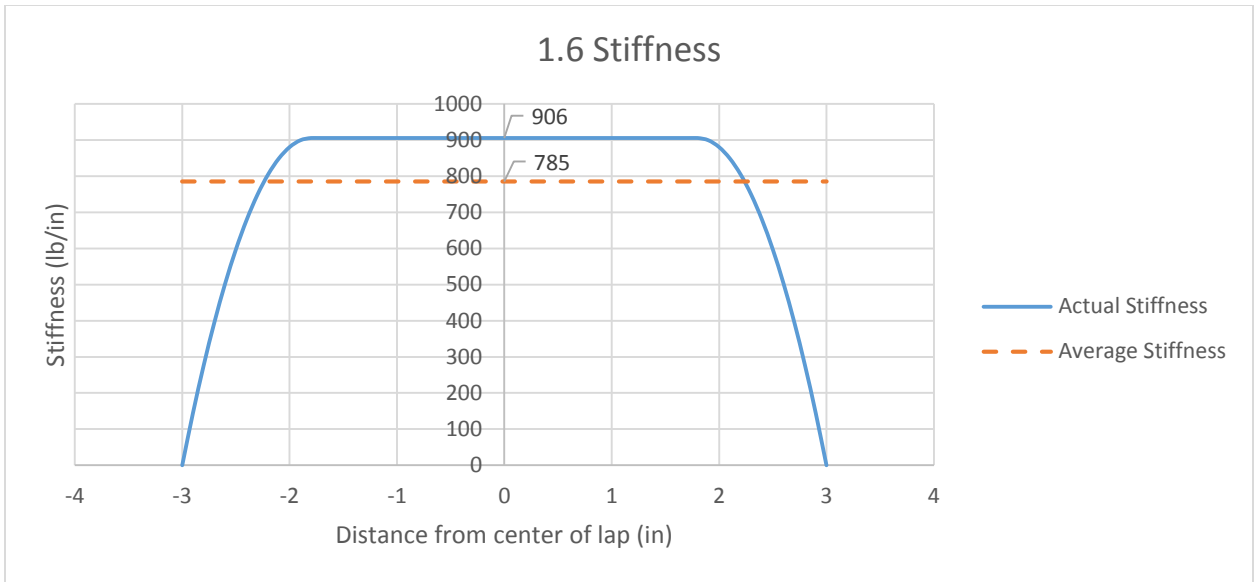
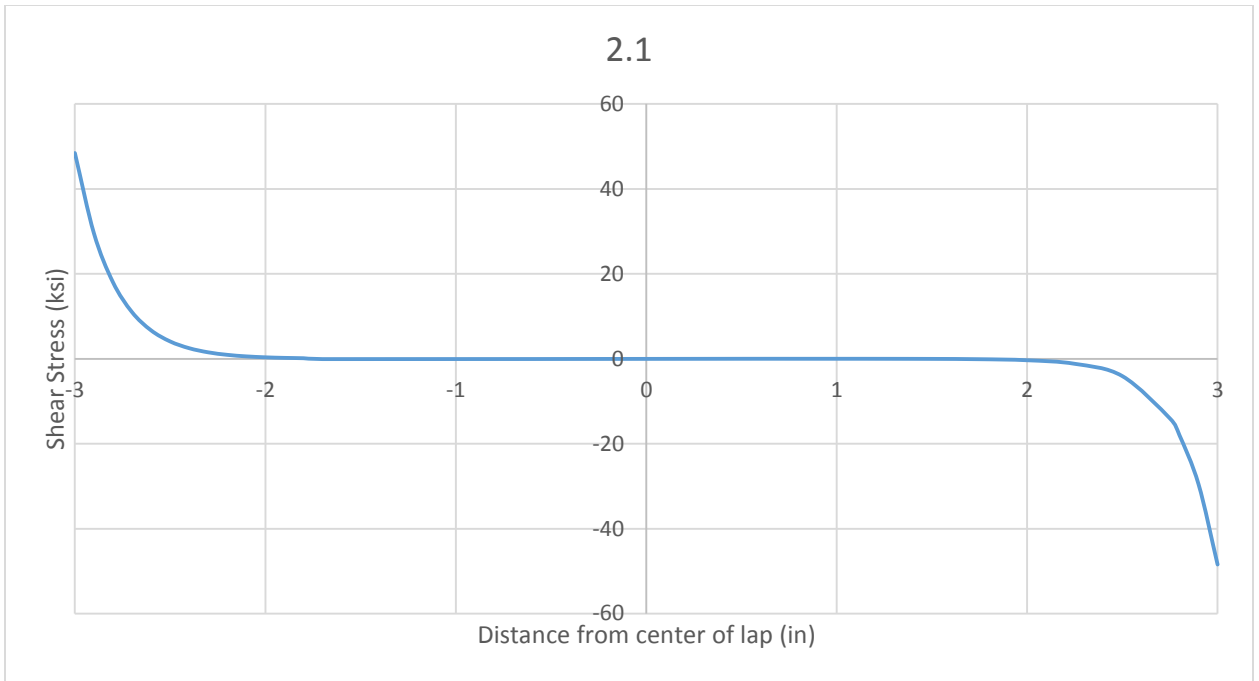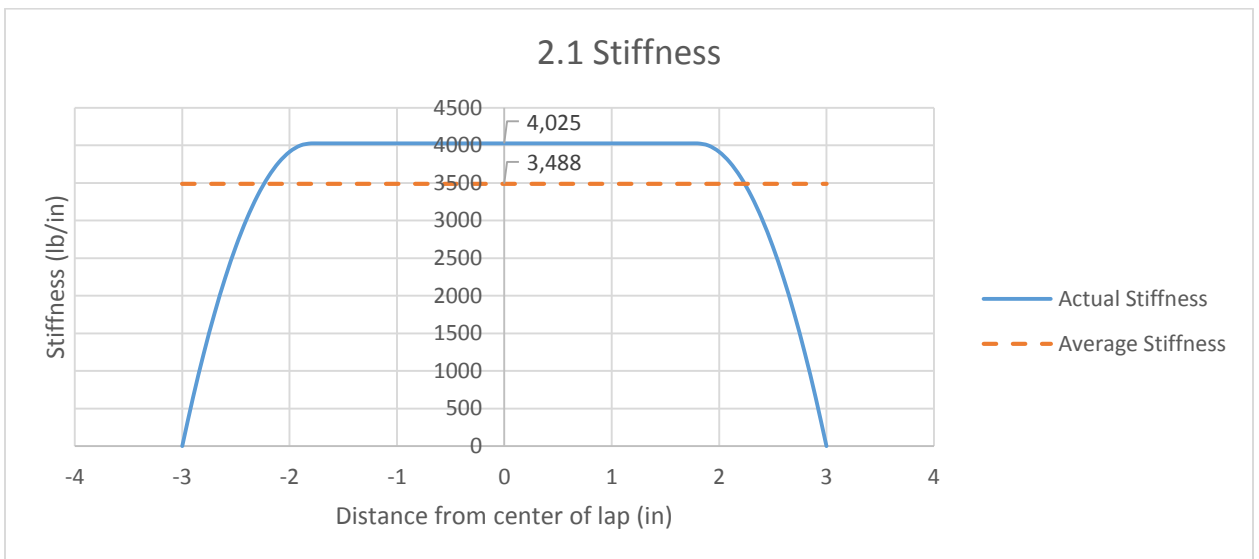**Figure 76. 1.6 joint stiffness**

## Specimen 2.1

| Specimen Properties: | | | | | | |
|---|---|---|---|---|---|---|
| $E_o =$ | 33,400.00 | ksi | | | | |
| $E_i =$ | 33,400.00 | ksi | $C_o =$ | 239.5 | kip/in.$^3$ | |
| $G_a =$ | 114.29 | ksi | $\lambda^2 =$ | 24.46 | in.$^{-2}$ | |
| $t_o =$ | 0.005045 | in. | $\lambda =$ | 4.95 | in.$^{-1}$ | |
| $t_i =$ | 0.005045 | in. | $C_o/\lambda^2 =$ | 9.79 | kip/in | |
| $t_a =$ | 0.036970 | in. | | | | |
| $P_x =$ | 39.169 | kip/in. | $P_x/n =$ | 9.79 | kip/in. | |
| $c = \pm$ | 3 | in. | | | | |
| $n =$ | 4 | | | | | |
| $E_a =$ | 419.00 | ksi | $C_o/\lambda =$ | 48,432.19 | psi | |
| $v_m =$ | 0.833 | | | | | |

**Figure 77. Properties to calculate specimen 2.1 stress distribution**
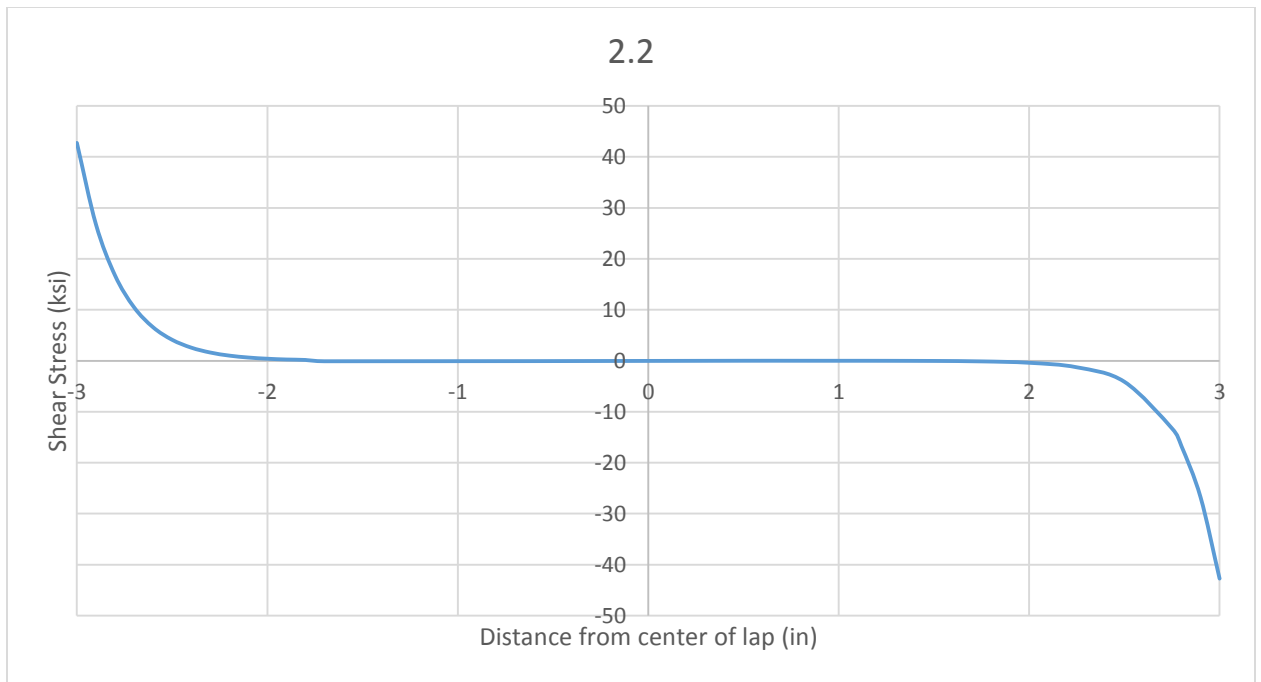
**Figure 78. 2.1 adhesive shear stress distribution**
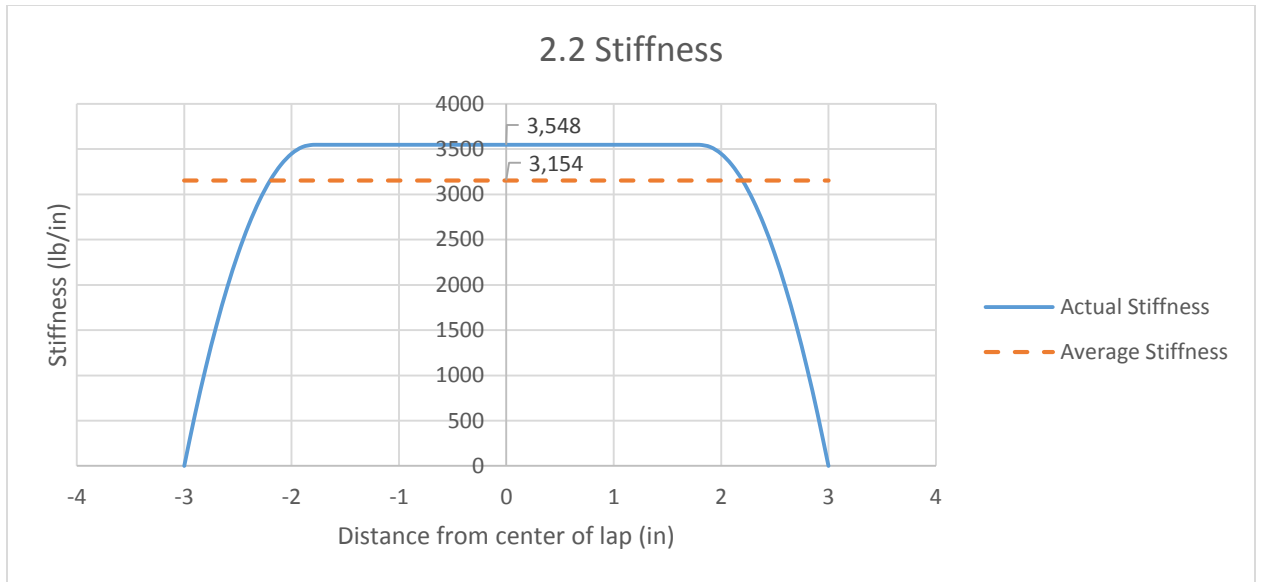


**Figure 79. 2.1 joint stiffness**

**Specimen 2.2**

| Specimen Properties: | | | | | |
|---|---|---|---|---|---|
| $E_o$ = | 33,400.00 ksi | | | | |
| $E_i$ = | 33,400.00 ksi | | $C_o$ = | 200.0 kip/in.$^3$ | |
| $G_a$ = | 113.37 ksi | | $\lambda^2$ = | 21.90 in.$^{-2}$ | |
| $t_o$ = | 0.005045 in. | | $\lambda$ = | 4.68 in.$^{-1}$ | |
| $t_i$ = | 0.005045 in. | | $C_o/\lambda^2$ = | 9.13 kip/in | |
| $t_a$ = | 0.040970 in. | | | | |
| $P_x$ = | 36.532 kip/in. | | $P_x/n$ = | 9.13 kip/in. | |
| c = ± | 3 in. | | | | |
| n = | 4 | | | | |
| $E_a$ = | 419.00 ksi | | $C_o/\lambda$ = | 42,735.33 psi | |
| $v_m$ = | 0.848 | | | | |

**Figure 80. Properties to calculate specimen 2.2 stress distribution**
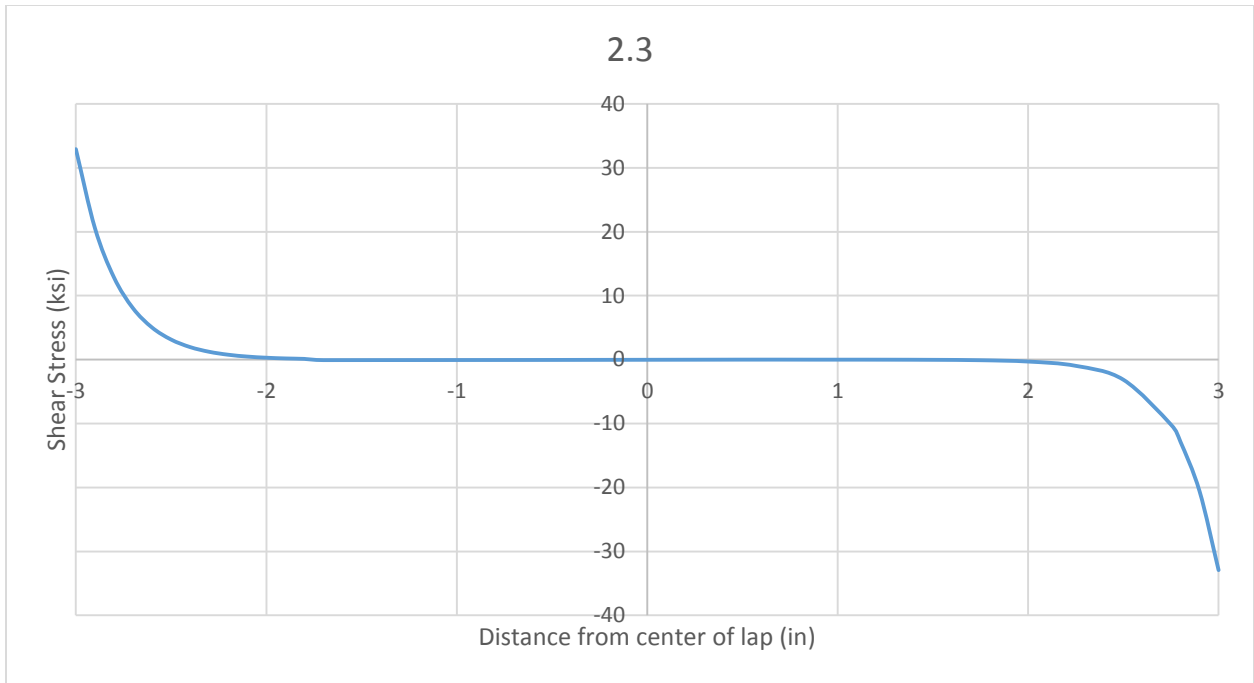


**Figure 81. 2.2 adhesive shear stress distribution**

71

## 2.2 Stiffness



**Figure 82. 2.2 joint stiffness**

**Specimen 2.3**

| Specimen Properties: | | | | | | | |
|---|---|---|---|---|---|---|---|
| $E_o$ = | 33,400.00 | ksi | | | | | |
| $E_i$ = | 33,400.00 | ksi | $C_o$ = | | 154.7 | kip/in.$^3$ | |
| $G_a$ = | 113.43 | ksi | $\lambda^2$ = | | 22.09 | in.$^{-2}$ | |
| $t_o$ = | 0.005045 | in. | $\lambda$ = | | 4.70 | in.$^{-1}$ | |
| $t_i$ = | 0.005045 | in. | $C_o/\lambda^2$ = | | 7.01 | kip/in | |
| $t_a$ = | 0.040637 | in. | | | | | |
| $P_x$ = | 28.02 | kip/in. | $P_x/n$ = | | 7.01 | kip/in. | |
| c = ± | 3 | in. | | | | | |
| n = | 4 | | | | | | |
| $E_a$ = | 419.00 | ksi | $C_o/\lambda$ = | | 32,920.88 | psi | |
| $v_m$ = | 0.847 | | | | | | |

**Figure 83. Properties to calculate specimen 2.3 stress distribution**

**Figure 84. 2.3 adhesive shear stress distribution**
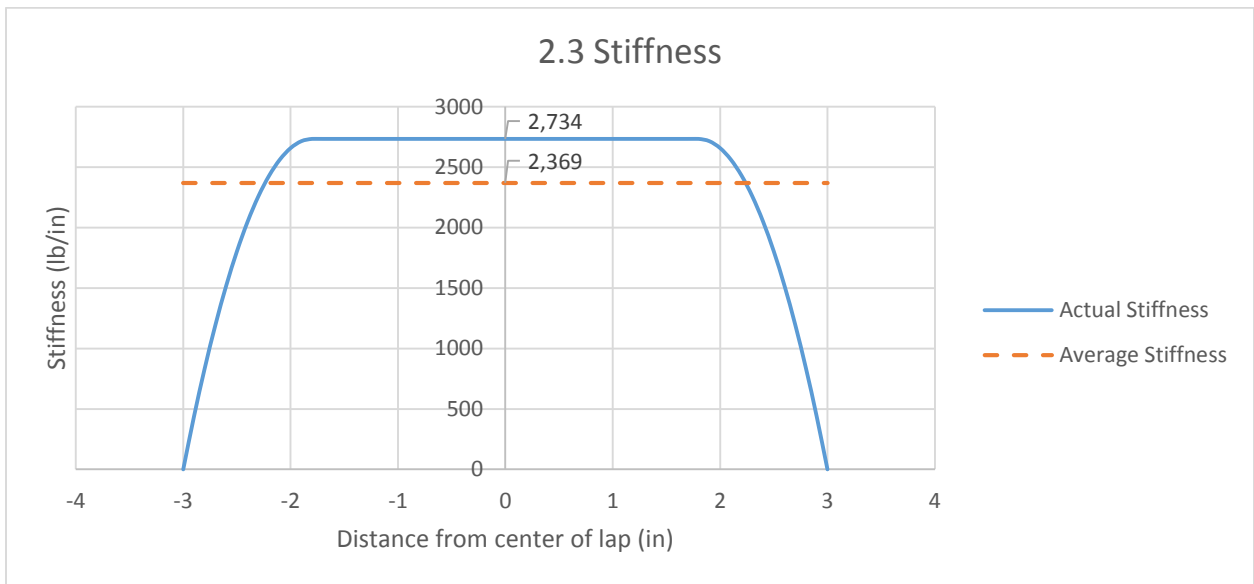


**Figure 85. 2.3 joint stiffness**